glutaraldehyde, 2,4,6-trinitrobenzenesulfonic acid, β-alanine, and a protein assay kit (# L8900) were purchased from Nacalai Tesque (Kyoto, Japan). The coupling agent, 1-ethyl-3-(3-dimethylaminopropyl) carbodiimide hydrochloride salt (EDC), was obtained from Dojindo Laboratories (Kumamoto, Japan). The CG was prepared by introducing ED to the carboxyl groups of low-molecular-weight gelatin (M.W. 3,100), as previously described [28]. Sodium borocaptate (Na_2 $^{10}B_{12}H_{11}SH$: BSH), was obtained from Stella Chemifa (Osaka, Japan).

Incorporation into HVJ-E

To incorporate plasmid DNA or BSH into HVJ-E, 10 μl of HVJ-E suspension (1.0×10^{10} particles) was added to 15 μl of 1% protamine sulfate, and this was mixed with plasmid DNA (200 μg) or BSH (6,667 μg boron) and 40 μl of 3% Tween-80 diluted with TE solution (10 mM Tris-HCl, pH 8.0, 1 mM EDTA). Qdot 655 ITK Carboxyl Quantum Dots (Qdot; Invitrogen, Carlsbad, CA, USA) were introduced into HVJ-E by electroporation (250 V, 750 μF). The mixture was centrifuged at 15,000 rpm for 15 min at 4°C. To remove the detergent and unincorporated plasmid DNA, BSH, or Qdot, the pellet was washed with 1 ml of balanced salt solution (10 mM Tris-HCl, pH 7.5, 137 mM NaCl, and 5.4 mM KCl), and the envelope vector was suspended in 1,000 μl of phosphate-buffered saline (PBS). To determine the ^{10}B concentration in the HVJ-E combined with BSH, the complex was digested with nitric acid solution at Bio Research (Hyogo, Japan) and assayed with inductively coupled plasma-atomic emission spectrometry (ICP-AES, ULTIMA2, Horiba Jobin Yvon, Kyoto, Japan).

Cationized Gelatin conjugate HVJ-E (CG-HVJ-E)

The CG-HVJ-E complex was formed by mixing the two materials in an aqueous solution. Briefly, 750 μg of CG was added to 150 μl of 0.1 M PBS (pH 7.4) containing 4.5×10^9 particles of HVJ-E. The solution was mixed by tapping several times. The solution was then incubated on ice for 15 min to form CG-HVJ-E. The CG-HVJ-E vector was purified by centrifugation as described above.

Zeta potential and particle size of HVJ-E compounds

The zeta potential of each HVJ-E complex (HVJ-E, CG-HVJ-E, HVJ-E-BSH, and CG-HVJ-E-BSH) was measured by an electrophoretic light scattering (ELS) assay (ELS-7000AS, Otsuka Electric Co. Ltd., Osaka, Japan) at 37°C with an electric field strength of 100 V/cm [29]. The particle size of each compound was measured by a dynamic light scattering (DLS) assay (Submicron Particle Analyzer N5, Beckman Coulter, Fullerton, CA, USA).

Transmission microscopy

Ultra-thin layers of HVJ-E, CG-HVJ-E, and CG-HVJ-E-BSH stained with 3% uranylacetate were examined with an electron microscope (H-7650 and S-800, Hitachi, Tokyo, Japan) to determine the particle size.

Hemagglutination assay

The hemagglutination assay was done in a 96-well round-bottom plate using 50 μl/well of a 0.5% suspension of chicken red blood cells (Nippon Bio-Test Laboratories, Tokyo, Japan) and 50 μl/well of an HVJ-E solution serially diluted with PBS [30].

Acute toxicity in normal mice

Each HVJ-E complex was administered by intra-cardiac injection (200 μl) into 8-12-week-old female C3H/HeN mice, which were monitored for 7 days for survival.

Blood chemistry monitoring after systemic administration of HVJ-E complexes

Indications of systemic injury were recorded, including serum levels of total bilirubin (T. Bil), aspartate aminotransferase (AST), and alanine aminotransferase (ALT) as markers of liver function, lactate dehydrogenase (LDH) and blood urea nitrogen (BUN) as markers of hemagglutination, and creatinine (Cr) as a marker of renal function. All marker levels were measured using an automated analyzing system (BML, Tokyo, Japan) at 24 and 48 hours and at 7 days after systemic administration of 4.5×10^9 HVJ-E particles.

Affinity of HVJ-E complexes to tumor cells and localization of Qdot carried in HVJ-E complexes

HVJ-E (1.5×10^9 particles) and CG (250 μg) were combined to produce CG-HVJ-E. LM8G5 cells (2×10^4) were seeded into each well of an 8-well Lab-tek chamber (Nalge Nunc International, Rochester, NY, USA) and cultured overnight. The cells were incubated with Qdot alone or Qdot with HVJ-E or CG-HVJ-E, at a concentration of 2.5×10^8 Qdot particles per well for 1 hour. The cells were washed twice with PBS and fixed with 4% paraformaldehyde. Hoechst 33342 (10 μM, Invitrogen) was used to stain the nuclei, and the cells were viewed with fluorescence microscopy (BX61, Olympus, Tokyo, Japan). To visualize the intracellular localization of the Qdot carried in the HVJ-E or CG-HVJ-E, the cells were stained with Hoechst 33342 for the nucleus and Alexa Fluor 488 phalloidin (Invitrogen) for the cytoplasm, and were viewed by confocal microscopy (Fluoview FV1000, Olympus).

Transfection efficiency of HVJ-E complexes into tumor cells

The various HVJ-E complexes were incubated with tumor cells to evaluate their transfection efficiency. LM8G5 cells (2×10^4) were seeded into each well of a 96-well plate, cultured overnight with 200 μl of culture medium, and washed with PBS. Each HVJ-E complex

with or without luciferase-expressing plasmids (50 μl; 1.5×10^9 particles) was incubated with tumor cells for 30 min, and then incubated for 30 min at 37°C. After washing twice with PBS, the cells were incubated with fresh medium for 24 hours and then lysed with Lysis Buffer (Promega, Madison, WI, USA). Luciferase activity in the cells was then measured with a Luciferase Assay kit (Promega) using a fluorescence plate reader (Mithras LB 940, Berthold Technologies, Bad Wildbad, Germany). The protein content of the samples was assayed by the Bradford method [31].

Accumulation and retention of BSH or CG-HVJ-E-BSH in tumor cells *in vitro*

Tumor cells of the LM8G5 cell line (1×10^6) were seeded in 75 cm^2 tissue culture flasks and were cultured overnight. The cells were then washed with PBS, 1 ml of BSH (20 μg boron/ml) or CG-HVJ-E-BSH (20 μg boron/ml) was added to each flask, and the mixture was incubated for 30 min at 37°C. The cells were then washed twice with PBS, and the ^{10}B concentration in the cells was immediately measured by ICP-AES (Horiba Jobin Yvon) as the initial ^{10}B value bound to the cells. Other flasks were incubated an additional 24-48 hours at 37°C and the cells were double-washed again before being tested for ^{10}B concentration, which was measured as the ^{10}B value.

Bio-distribution of BSH or CG-HVJ-E-BSH in normal or liver tumor-bearing mice

Mice were injected with 200 μl of BSH (35 μg boron/g) or 200 μl of CG-HVJ-E-BSH (1.2 μg boron/g), administered into the general circulation. At 1, 24, or 48 hours after the injection, mice were sacrificed and peripheral blood samples collected. The lung, liver, kidney and spleen were removed after whole-body perfusion with heparinized saline, and weighted. The extracted tissues were digested with the M-Per mammalian protein extraction reagent (Pierce Chemical Co., Rockford, IL, USA) and ultrasonic homogenizer (H3-350, Kawajiri Machinery, Hyogo, Japan), and the ^{10}B concentration in each sample was measured by ICP-AES (Horiba Jobin Yvon). The ^{10}B accumulation into each organ was calculated as the percentage of ^{10}B per weight of each organ.

Neutron capture autoradiography imaging of murine liver sections after BSH or CG-HVJ-E-BSH administration

Mice bearing liver tumors were given either 35 μg boron/g of BSH or 1.2 μg boron/g of CG-HVJ-E-BSH, administered into the general circulation. The mice were sacrificed 1 hour after BSH administration or 24 hours after CG-HVJ-E-BSH administration. The liver was removed after whole-body perfusion with heparinized saline. Frozen 16-μm-thick liver sections were mounted on Baryotrak-P detector plates (Nagase-Landauer, Tokyo, Japan) and air-dried for 60 min. The samples were exposed to thermal neutrons at a rate of 2.1×10^{13} neutrons/$m^2 \cdot s^1$ for 1 hour at the Japan Research Reactor 4 (JRR-4). For α-auto-radiographic imaging, the detector plates were etched in 7 N NaOH at 70°C for 2 hours to reveal the proton tracks produced by the boron neutron capture reaction [32]. The number of α particles per 10,000 μm^2 in each section was counted using VH Analyzer software (Biozero, Keyence, Osaka, Japan).

Antitumor efficacy of BNCT for murine liver tumors with BSH or CG-HVJ-E-BSH

Mice bearing liver tumors were irradiated with a thermal neutron beam at the JRR-4 8 days after tumor cell inoculation. The mice were given 1.2 μg boron/g of CG-HVJ-E-BSH 24 hours before irradiation treatment, or 35 μg boron/g of BSH 1 hour before irradiation treatment, administered into the general circulation. The mice were then set the acrylic stand, and irradiated for 17 min at the Japan Research Reactor 4 (JRR-4). Neutron irradiation was performed in a single fraction using an thermal beam mode I of JRR-4. In the in-air beam characteristics, thermal neutron flux and the γ-ray absorbed dose were 2.1×10^{13} neutrons/$m^2 \cdot s^1$ and 3.6 Sv/h at a reactor power of 3.5 MW, respectively. To evaluate the effect of BNCT treatment on the liver tumors, the mice were sacrificed 6 days after irradiation, and the livers removed, weighed, and evaluated for pathologic changes. In a separate experiment, 1.2 μg boron/g of BSH or 1.3 μg boron/g of CG-HVJ-E-BSH was administered, the mice were either irradiated or not, and their survival time after irradiation was recorded.

Statistical analyses

Student's *t*-test was used to determine whether the differences between the various groups were significant. Differences between groups in the survival experiment were determined using the Kaplan-Meier log-rank test. A *p*-value of less than 0.05 was considered statistically significant.

Results

CG-HVJ-E characteristics

SDS-PAGE results confirmed that when mixed and centrifuged with HVJ-E, the CG bound to HVJ-E in a dose-dependent manner within a certain range (data not shown). The optimal ratio of CG to HVJ-E, in which the CG-HVJ-E containing luciferase plasmid was transferred most efficiently into LM8G5 cells (data not shown), was identified as 1 μg to 6.0×10^6 particles, and the zeta potential and particle size of the resulting CG-HVJ-E conjugate was measured (Table 1). CG- HVJ-E was

Table 1 Zeta potential and particle sizes of each HVJ-E complex

Complex	Apparent molecular size (nm)	Zeta potential (mV)
HVJ-E	293 ± 32	-25 ± 1
CG-HVJ-E	297 ± 21	-15 ± 3
HVJ-E-BSH	448 ± 144	-28 ± 1
CG-HVJ-E-BSH	494 ± 196	-19 ± 2

more positive (-14.7 mV) than HVJ-E (-25.1 mV). The form and size of these particles were estimated by using Transmission Electron Microscopy (TEM) and Scanning Electron Microscopy (SEM). HVJ-E, CG-HVJ-E, and CG-HVJ-E-BSH were approximately 300, 300, and 500 nm in diameter, respectively, as measured by TEM (Additional file 1, Figure S1). The DLS assay results were similar (data not shown). Therefore, these data are able to give an estimate that incorporating BSH into the HVJ-E complexes made them larger and slightly more positive than either HVJ-E or CG-HVJ-E.

CG-HVJ-E had less hemagglutination activity in vitro and was less toxic than HVJ-E in mice

Hemagglutination is caused by hemagglutinin-neuraminidase (HN) protein on the HVJ-E membrane [33]. The hemagglutination of chicken blood cells by CG-HVJ-E was approximately half that of HVJ-E (data not shown). The acute toxicity was determined by administering various concentrations of HVJ-E or CG-HVJ-E to normal mice and monitoring their survival over 7 days; the 100% survival dosage of CG-HVJ-E (6.0×10^9 particles) was higher than that of HVJ-E (4.5×10^9 particles). Blood tests done 24 hours after the administration of 4.5×10^9 particles of HVJ-E or 4.5×10^9 particles of CG-HVJ-E showed that blood chemistry markers in the CG-HVJ-E-treated mice were almost within the normal range, while those in the HVJ-E-treated mice were significantly higher (Figure 1). These levels peaked 24 hours after administration in mice treated with HVJ-E, and became normal at 7 days (data not shown).

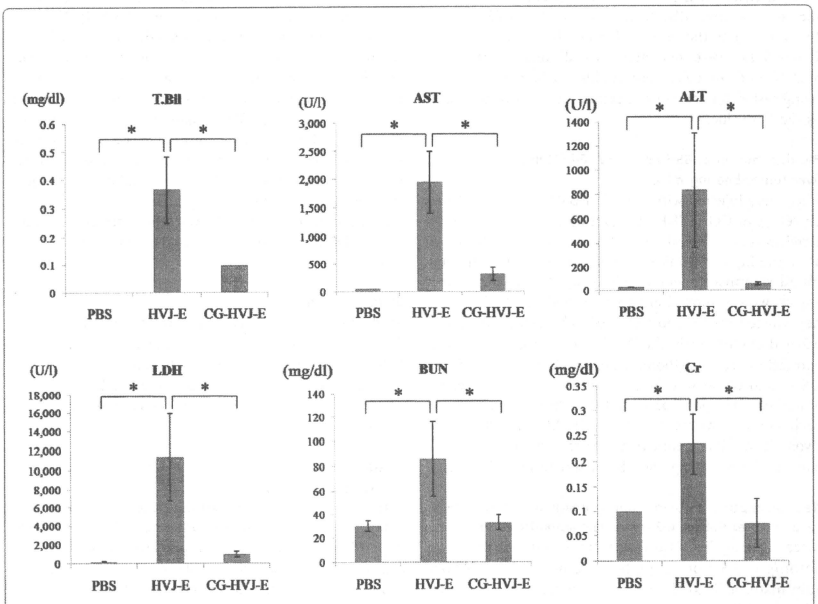

Figure 1 Blood chemistry tests 24 hours after HVJ-E and CG-HVJ-E administration into normal mice. Blood markers (T.Bil, AST, ALT, LDH, BUN, and Cr) in normal mice tested 24 hours after intra-cardiac injection of PBS, HVJ-E or CG-HVJ-E. * $p < 0.05$. Results shown are the means ± SD (n = 4).

High affinity and infusion ability of CG-HVJ-E in tumor cells

CG-HVJ-E containing Qdot had a higher affinity for tumor cells than Qdot alone or HVJ-E containing Qdot (Figure 2A). CG-HVJ-E containing Qdot was taken into the cytoplasm, and some Qdots were localized to the nuclei, as seen by confocal microscopy (Figure 2B).

CG-HVJ-E transfection into tumor cells *in vitro* was highly efficient

CG-HVJ-E's *in vitro* transfection efficiency into tumor cells was 4 times greater than that of HVJ-E, as assessed by a luciferase assay, and it was not cytotoxic (Figure 2C). The enhanced transfection efficiency of CG-HVJ-E was also observed in another tumor cell line (CT26: murine colon cancer, data not shown).

CG-HVJ-E-BSH increased ^{10}B accumulation and retention in tumor cells *in vitro* compared to BSH

The concentration of ^{10}B was significantly higher in cells incubated with CG-HVJ-E-BSH than in those incubated with BSH ($p < 0.05$). The ^{10}B levels gradually decreased in both cell groups, but the levels were significantly higher in the cells incubated with CG-HVJ-E-BSH than

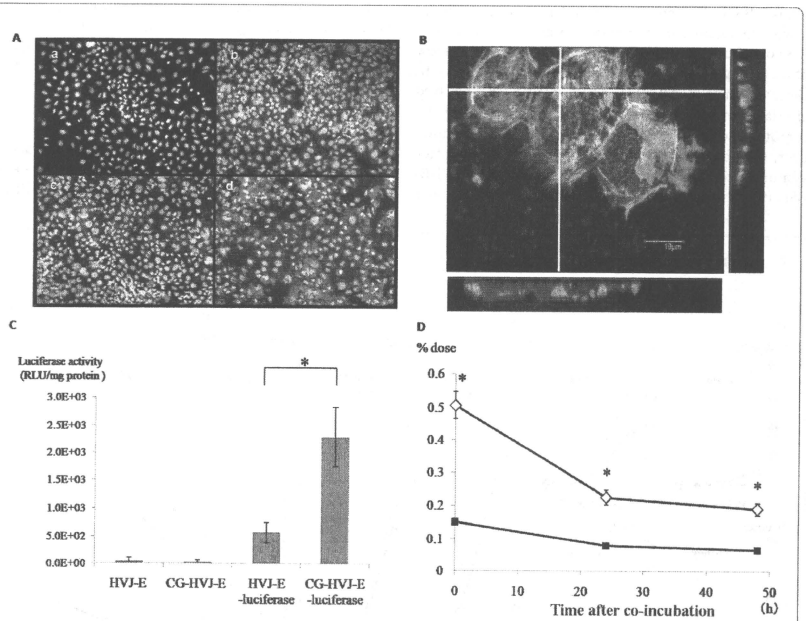

Figure 2 Affinity of CG-HVJ-E for tumor cells and the intracellular uptake of molecules incorporated into HVJ-E. A) Affinity of HVJ-E and CG-HVJ-E for tumor cells. LM8G5 cells were incubated alone (a), or with Qdot (b), HVJ-E-Qdot (c), or CG-HVJ-E-Qdot (d) for 60 min in a Lab-tek chamber slide and examined for Qdot (red) and Hoechst 33342 (blue) by fluorescence microscopy. Representative views are shown. B) Intracellular localization of Qdot transported by CG-HVJ-E. Tumor cells were incubated with CG-HVJ-E-Qdot (orange) and stained with Hoechst 33342 (blue) and Alexa Fluor 488 phalloidin (green). Image shows 3-dimensional analysis with confocal microscopy. C) Luciferase activity in tumor cells transfected with HVJ-E or CG-HVJ-E. Cells were cultured for 30 min with HVJ-E or CG-HVJ-E containing a luciferase-expressing plasmid. Luciferase activity was measured 24 hours later to evaluate the transfection efficiency. Results are shown as means ± SD (n = 4). Similar results were obtained in three experiments. * $p < 0.05$. D) ^{10}B accumulation and retention in tumor cells *in vitro*. Cells were incubated with 20 μg boron/ml of BSH or CG-HVJ-E-BSH for 30 min, then washed twice with PBS, and the ^{10}B concentration was measured by ICP-AES. Separately, cells were incubated in the same manner, but after washing, were incubated in medium without BSH for 24 or 48 hours before testing for ^{10}B concentration as described above. The horizontal axis shows time after co-incubation. The vertical axis shows the percent of the administered dose (% dose) of CG-HVJ-E-BSH (open diamond) or BSH (solid square). Results shown are the means ± S.D. (n = 3). * $p < 0.05$.

in those with BSH for at least 48 hours after incubation (Figure 2D). These results indicate that CG-HVJ-E-BSH binds rapidly to tumor cells and that the ^{10}B contained in CG-HVJ-E-BSH is internalized into the cytoplasm or the nucleus. Adding CG-HVJ-E-BSH to tumor cells *in vitro* resulted in sufficient ^{10}B accumulation and retention in the cells to be useful for BNCT.

BSH incorporated into CG-HVJ-E accumulated in liver tumors and rapidly disappeared from normal tissues in tumor-bearing mice

In normal mice, the ^{10}B concentration in the liver 1 hour after administration was higher with BSH than with CG-HVJ-E-BSH. The concentration of both compounds started to decrease by 48 hours after administration. The ^{10}B concentration in the lung, kidney, and spleen was low at all time points with both compounds (Figure 3A). In the liver tumor model, BSH and CG-HVJ-E-BSH behaved similarly in the normal liver tissue surrounding the tumors (Figure 3B, middle panel). In the tumors, however, the concentration of ^{10}B at 1 and 24 hours after administration was significantly higher with CG-HVJ-E-BSH (34.76 and 10.71% dose/g) than with BSH (2.21 and 2.29% dose/g) (Figure 3B, left panel). In the bloodstream, the ^{10}B concentration at 1 hour after administration tended to be higher with CG-HVJ-E-BSH (20.9% dose/ml) than with BSH (7.96% dose/ml), despite the lower quantity of ^{10}B administered with both boron compounds (1.2 μg boron/g). From 24 hours after administration and onward, the concentration of ^{10}B from both compounds was the same (Figure 3B, right panel).

Tumor/Normal liver ^{10}B ratio in murine liver tumors was greater with CG-HVJ-E-BSH

The Tumor/Normal (T/N) liver ^{10}B ratio with CG-HVJ-E-BSH was significantly higher than with BSH from 1 to 48 hours after administration ($p < 0.05$), with a peak difference at 24 hours ($p < 0.05$; Figure 3C). The Tumor/Blood ^{10}B ratio of CG-HVJ-E-BSH also remained higher than that of BSH from 1 to 48 hours after administration (data not shown).

CG-HVJ-E-BSH improved the T/N ^{10}B ratio in neutron capture autoradiography images of murine liver tumors

Neutron capture autoradiography (NCAR) was performed after BSH (35 μg boron/g) or CG-HVJ-E-BSH

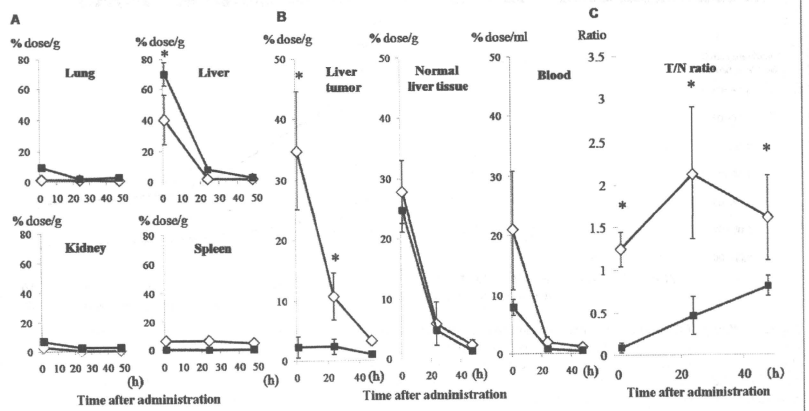

Figure 3 Bio-distribution of ^{10}B in mice with normal liver or with liver tumors. A) Time course of organ (lung, liver, kidney, and spleen) uptake of ^{10}B delivered by 1.2 μg boron/g of BSH or CG-HVJ-E-BSH in normal mice. B) Time course of tumor accumulation (left panel), liver uptake (middle panel), and blood residence (right panel) of ^{10}B delivered by 1.2 μg boron/g of BSH or CG-HVJ-E-BSH in tumor-bearing mice. The horizontal axis shows the time after administration. The vertical axis shows the percent of the administered dose per gram of tissue (% dose/g). C) Time course of the Tumor-to-Normal liver tissue (T/N) ^{10}B concentration ratio for CG-HVJ-E-BSH (open diamond) or BSH solution (solid square). Data are expressed as the mean ± S.D. ($n = 3$). * $p < 0.05$ compared with BSH.

(1.2 μg boron/g) was injected into mice bearing liver tumors. The ^{10}B particle count in the BSH- and CG-HVJ-E-BSH-treated livers are shown in Figure 4B and 4C. The T/N ratio 1 hour after BSH administration was 0.12, and that for CG-HVJ-E-BSH at 24 hours after administration was 2.76 (Figure 4D), which is similar to the values obtained in the bio-distribution study. It is of interest that the T/N ^{10}B ratio was higher with CG-HVJ-E-BSH, even though the actual quantity of ^{10}B was 30 times greater in the BSH dosage. The number of α particles with CG-HVJ-E (415 ± 35) was similar to that of BSH (451 ± 107) in the liver tumor sections (Figure 4A).

BNCT with CG-HVJ-E-BSH inhibited tumor growth, preserved the normal surrounding liver tissue, and prolonged survival time in the murine liver tumor model

To evaluate the use of BNCT with CG-HVJ-E-BSH for murine liver tumors, BNCT was performed on mice bearing LM8G5 liver tumors. To assess the T/N ratio of CG-HVJ-E-BSH, BNCT was performed 24 hours after CG-HVJ-E-BSH administration or 1 hour after BSH administration [2,4]. We first evaluated the anti-tumor efficacy at 14 days after tumor cell inoculation, because up to that time, the tumor-bearing mice were severely damaged by the radical spread of tumors (about 50% of the untreated mice were dead). Therefore, we sacrificed the tumor-bearing mice that were alive until that time to evaluate the efficacy of BNCT.

BNCT with CG-HVJ-E-BSH (1.2 μg boron/g) inhibited the local growth of liver metastases as much as BNCT with BSH (35 μg boron/g). This dosage of BSH was determined from the clinical dose for BNCT for various malignant tumors, and effectively contained 35 times the ^{10}B that was present in the CG-HVJ-E-BSH dosage (Figure 5A, B). Some histological damage, which appeared, for example as fractionated or vacuolated

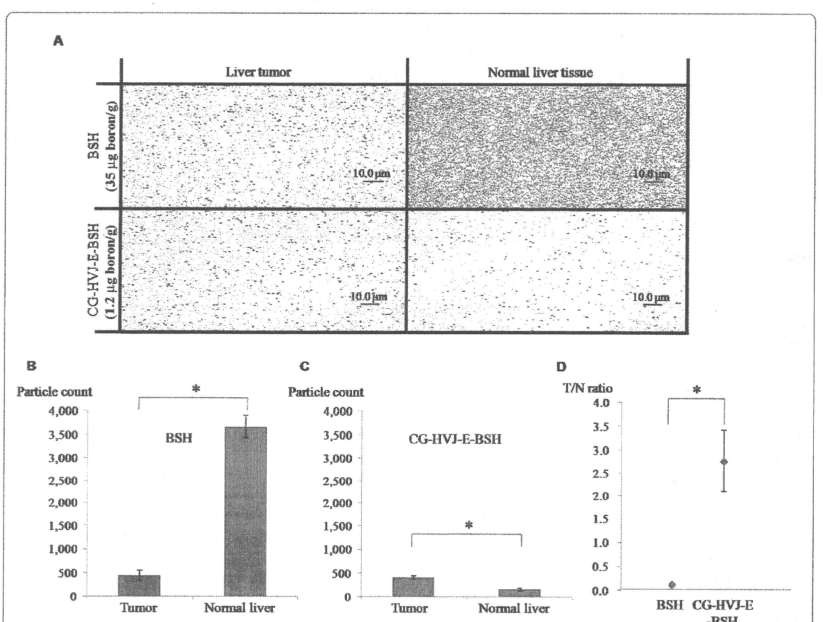

Figure 4 Neutron capture radiographic image in murine liver sections after administration of BSH or CG-HVJ-E-BSH. Liver sections from tumor-bearing mice were prepared and frozen 1 hour after BSH (35 μg boron/g) injection or 24 hours after CG-HVJ-E-BSH (1.2 μg boron/g) injection. The sections were placed on CR-39 detector plates and exposed to thermal neutrons (2.1×10^{13} neutrons/m^2·s^1) for 1 hour. A) The number of α particles per 10,000 μm^2 section was counted by VH Analyzer software after NaOH etching. B) The number of α particles per 10,000 μm^2 section of BSH or C) of CG-HVJ-E-BSH (n = 3). D) Tumor-to-normal liver tissue (T/N) ratio for the number of α particles.

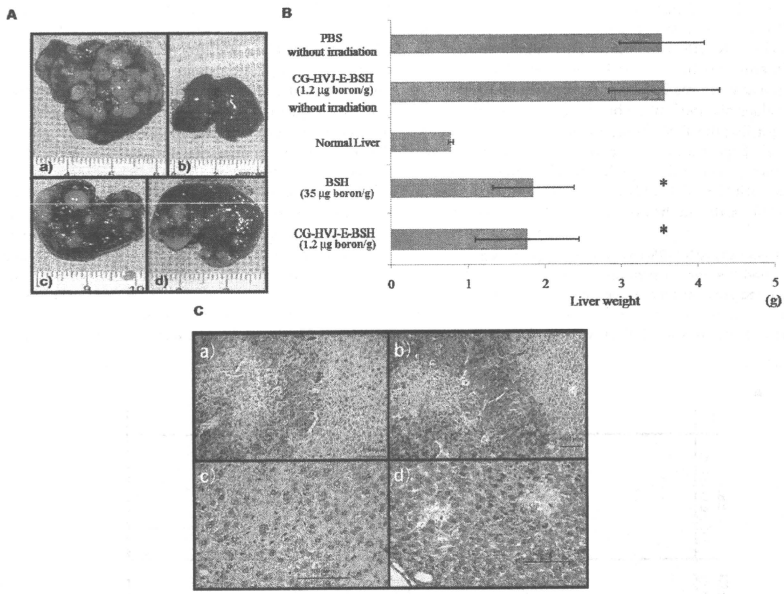

Figure 5 Anti-tumor efficacy of BNCT in mice with liver tumors. C3H/HeN mice were given an intra-portal injection of LM8G5 cells (1×10^6 cells) on day 0. Mice were given a single intra-cardiac injection of CG-HVJ-E-BSH (1.2 μg boron/g) 24 hours before irradiation, or BSH (35 μg boron/g) 1 hour before irradiation. PBS and CG-HVJ-E-BSH solution were administered without neutron irradiation as a control. After irradiation on day 8, mice were sacrificed on day 14 to determine the BNCT efficacy on tumor metastasis. A) Macroscopic views (a) of the liver with tumors after administration of PBS; (b) normal liver; (c) liver with tumors after BNCT with BSH, and (d) liver with tumors after BNCT with CG-HVJ-E. B) Liver weight after BNCT. * $p < 0.05$ compared with PBS or CG-HVJ-E without irradiation. (each group n = 4). C) Representative light microscopic views of liver tumor tissue (upper panels, low magnification) or normal liver tissue (lower panels, high magnification) 6 days after BNCT with CG-HVJ-E-BSH (1.2 μg boron/g) (a, c) or BSH (35 μg boron/g) (b, d). Sections are stained with hematoxylin-eosin. Bar: 100 μm.

cells, was observed in both the tumor mass and in the normal liver tissue after BNCT with BSH (35 μg boron/g) (Figure 5C-b, d). In contrast, little histological damage was detected in the normal liver tissue surrounding the tumors after BNCT with CG-HVJ-E-BSH (Figure 5C-a, d). We originally thought that the damage to the liver might have been influenced by the longer survival time of mice treated with BSH and BNCT; however, the survival rate of these mice at 14 days after tumor cell inoculation was 37.5% (Additional file 2, Figure S2). This survival time was shorter than that of the untreated tumor-bearing mice. As we were not able to be certain if this dosage of BSH was a clinical equivalent, we used a dose of 1.3 μg boron/g of BSH to evaluate the survival time after BNCT, compared to a dose of 1.2 μg boron/g of CG-HVJ-E-BSH.

Finally, we compared the effectiveness of BNCT against tumors when used with BSH or CG-HVJ-E-BSH, in terms of survival after BNCT. With the assumption that the survival time of tumor-bearing mice after BNCT with a high dose of BSH (35 μg boron/g) was affected by normal liver damage as well as anti-tumor efficacy, both compounds were administered at dosages with similar ^{10}B concentrations (CG-HVJ-E-BSH, 1.2 μg boron/g or BSH,1.3 μg boron/g) into mice bearing liver tumors at 24 hours or 1 hour before irradiation, respectively. Irradiation was performed 8 days after the tumor cell inoculation, and the survival of the mice assessed.

CG-HVJ-E-BSH was most effective in increasing the mean survival time of mice bearing liver tumors compared with the other groups ($p < 0.005$; Additional file 2, Figure S2). We observed little histological damage in the normal liver tissues 6 days after BNCT with the lower dose of BSH (1.3 μg boron/g) besides the damage that was already present in the tumor mass (Additional file 3, Figure S3).

Discussion

With the goal of creating a novel BSH vector for effective BNCT, we chose HVJ-E because of its strong fusion ability, its effectiveness as a vehicle for delivering various drugs and genes, and its ability to stimulate an immune response against tumors in local cancer therapy [23]. Clinical trials of locally administered HVJ-E for patients with advanced malignant melanoma are underway in Japan. Although HVJ-E is not suitable for systemic administration because of its strong hemagglutinating activity, it has been reported that combining HVJ-E with 5,000-kDa cationized gelatin greatly improves its stability in the bloodstream [25]. In this study, we developed CG-HVJ-E combined with BSH, which can be administered into the general circulation, unlike HVJ-E, and confirmed its bio-distribution.

We compared the safety and efficacy of CG-HVJ-E-BSH in BNCT with that of BSH, using a murine model for liver tumors. For systemic administration, we developed a smaller CG-HVJ-E with a lower molecular weight (3,300 kDa) CG compared with the previously used CG-HVJ-E, which had a particle diameter of 777 nm [25]. We found that this CG-HVJ-E could be safely administered systemically in mice, with reduced toxicity and hemagglutination compared to HVJ-E (Figure 1). In the bio-distribution test using normal mice, both BSH and CG-HVJ-E-BSH accumulated in the liver immediately, but almost all of the ^{10}B had disappeared from the normal liver 48 hours later (Figure 3A). In liver tumors, however, CG-HVJ-E-BSH accumulation was greater than that of BSH although the boron proceeding from CG-HVJ-E-BSH was 35 times higher than that of BSH (Figure 3B); accordingly, the CG-HVJ-E-BSH T/N ratio was significantly higher than that of BSH in tumor-bearing mice, particularly at 24 hours after administration (Figure 3C). Neutron capture autoradiography revealed a higher T/N ^{10}B ratio with CG-HVJ-E-BSH than with BSH 1 hour after administration, despite the 35-fold-higher quantity of ^{10}B contained in the BSH dosage (Figure 4).

In our experiments, BNCT was performed 1 hour after BSH administration, because it followed the reported procedure for the clinical use of BNCT for liver tumors [9], and there was little difference between the T/N ratio an hour after administration and the ratio over the next 24 hours (Figure 3C). This was due to the protracted circulating time of CG-HVJ-E-BSH in the bloodstream. Therefore, this complex accumulated in the tumor by the enhanced permeability and retention (EPR) effect [34]. In fact, the particle size of the CG-HVJ-E-BSH was suitable for the EPR effect (Table 1) [35]. Another reason for this finding was that CG-HVJ-E has a high affinity and high fusion ability for tumor cells (Figure 2A, B, C). Although ^{10}B was taken up by the tumor cells over time, a large number of CG-HVJ-E-BSH molecules were incorporated into the tumor cells immediately, and high ^{10}B concentrations were maintained much longer with CG-HVJ-E-BSH than with BSH (Figure 2D). The mechanism for the preferential affinity of CG-HVJ-E to tumor cells as compared with HVJ-E has not been clarified, but it has been reported that when HVJ-E is conjugated with cationized gelatin, the transfection efficiency improves without a loss of cell fusion ability [25]. Therefore, the efficacy of CG-HVJ-E-BSH was similar to the 35-fold higher dose of ^{10}B as BSH for suppressing the spread of tumor cells without normal liver injury (Figure 5A, B, C).

When used in BNCT, the CG-HVJ-E-BSH significantly increased the survival time over BSH at an equivalent ^{10}B dosage (Additional file 2, Figure S2). Generally, BSH is rarely transferred into the cytoplasm and, once there, is easily removed [36]. On the other hand, CG-HVJ-E-BSH was highly selective for tumor cells and showed both strong fusion ability and the ability to transfer into the tumor cell nucleus. As a result, CG-HVJ-E-BSH improved the effectiveness of BNCT because the ^{10}B was highly concentrated and retained in the nuclei of the tumor cells (Figure 2B, C), where its cytotoxicity was much higher than that of ^{10}B bound to the tumor cell surface [14,37,38].

Moreover, HVJ-E has the potential to induce a bystander effect, so that CG-HVJ-E-BSH could be incorporated into vicinal cells through gap junctions. It is possible that BNCT with CG-HVJ-E-BSH induces a synergistic effect, resulting in a greater destruction of vicinal tumor cells than is seen with BNCT with BSH, which induces a bystander effect that generates hereditary abnormalities in vicinal cells [39].

We chose multiple liver tumors as a target for evaluating the effectiveness of BNCT with CG-HVJ-E-BSH, because BNCT for multiple liver tumors has not gained popularity and the T/N ratio needs to be improved for deep-site tumors. In the absence of liver function disorders, the response of multiple liver tumors is thought to be a good indication of BNCT effectiveness. In this report, we treated mice bearing liver tumors with BNCT [27] after establishing the presence of tumors of several millimeters in diameter. This murine model appears to reflect the clinical stage that we targeted. BNCT with BSH is not indicated for multiple liver tumors in clinical

settings and is only at the experimental stage [9,10]. BNCT was significantly more effective against liver tumors when used with CG-HVJ-E-BSH than with BSH, and normal liver tissue was not injured. The limited injury to normal liver tissue makes more than one BNCT irradiation possible, which is likely to increase the therapeutic potential. However, in these experiments, only one irradiation was done. With regard to BNCT with BSH for clinical liver tumors at deep sites, the required T/N ^{10}B ratio is over 15 [36,40]. Moreover, the human trunk is much thicker than the murine trunk. Therefore, for BNCT with CG-HVJ-E-BSH to become an established, effective clinical procedure, further improvements are needed not only in the drug-delivery system, but also in the vessel-selective delivery [41] because of the attenuation of neutron beams directed toward deep lesions.

Our trial of BNCT for multiple liver tumors at deep sites should forward its development to treat other deep-site tumors, such as pancreatic cancer and malignant mesothelioma [42-44], and further the investigation into BNCT and HVJ-E. However, some problems need to be resolved in future experiments, particularly with regard to improving the incorporation of ^{10}B into the HVJ-E.

It has been reported that locally administered HVJ-E induces immuno-responses against tumors [23, 24], and effectively transports antitumor drugs [22,45]. Our experiments included a single administration of HVJ-E, which did not appear to have an anti-tumor effect unless accompanied by irradiation (Figure 5B, Additional file 2, Figure S2). However, the fractionated administration of HVJ-E, as is used for other vaccinations, might be possible. To address the limitations of this novel HVJ-E BSH, investigations into concurrent chemo-radiation therapy, fractionated administration with or without ^{10}B, and conjugating with ligands for tumor-specific molecules should be performed.

In summary, we developed a form of CG-HVJ-E that could be administered into the general circulation and had both high tumor selectivity and high retention in tumor cells. This vector, when combined with BSH, improved the efficacy of BNCT for multiple liver tumors *in vivo*. Therefore, CG-HVJ-E holds potential for a drug delivery system with clinical applications for cancer therapy.

Additional material

Additional file 1: Figure S1. Transmission electron microscope photographs of HVJ-E complexes. (A) HVJ-E, (B) CG-HVJ-E, and (C) CG-HVJ-E-BSH. Bar: 200 nm.

Additional file 2: Figure S2. Survival of mice treated with BNCT. Mice were given a single intra-cardiac injection of CG-HVJ-E-BSH (1.2 μg boron/g) 24 hours before irradiation, or BSH (1.3 μg boron/g) 1 hour before irradiation. PBS and CG-HVJ-E-BSH were administered without irradiation as a control. The mean survival time of the mice that received the BNCT treatment with CG-HVJ-E-BSH was significantly longer than that of the other groups (n = 4). * $p < 0.005$ (PBS without neutron irradiation, 1.3 μg boron/g of BSH with neutron irradiation, 1.2 μg boron/g of CG-HVJ-E-BSH without neutron irradiation vs. 1.2 μg boron/g of CG-HVJ-E-BSH with neutron irradiation).

Additional file 3: Figure S3. Representative light microscopy views of the liver tumor (A) and normal liver tissue (B) 6 days after BNCT with a low dose of BSH (1.3 μg boron/g). Tissues were stained with hematoxylin-eosin. Bar: 100 μm.

Abbreviations

BNCT: Boron Neutron Capture Therapy; BSH: sodium borocaptate; HVJ-E: Hemagglutinating Virus of Japan Envelope.

Acknowledgements

This work was supported in part by a grant for research and development of a Fixed Field Alternating Gradient Accelerator and DDS for BNCT from the New Energy and Industrial Technology Development Organization (NEDO), a Health Labour Science Research Grant from the Ministry of Health, Labour and Welfare of Japan, and a grant-in-Aid for Exploratory Research from the Ministry of Education, Culture, Sports, Science and Technology (MEXT).

Author details

[1]Department of Surgery, Osaka University Graduate School of Medicine, Osaka, Japan. [2]Medical Center for Translational Research, Osaka University Hospital, Osaka, Japan. [3]Particle Radiation Oncology Research Center Laboratory, Research Reactor Institute, Kyoto University, Osaka, Japan. [4]Department of Agriculture, Osaka Prefectural University, Osaka, Japan. [5]Department of Biomaterials, Institute for Frontier Medical Sciences, Kyoto University, Kyoto, Japan. [6]Division of Gene Therapy Science, Osaka University Graduate School of Medicine, Osaka, Japan. [7]Health Care Economics and Industrial Policy, Osaka University Graduate School of Medicine, Osaka Japan.

Authors' contributions

HF carried out the study, and contributed to the conception of the manuscript and the interpretations of the data. AM, HK, MS, MS, AT, and YT participated in the design of the study. YD, MK, and KO provided some intellectual recommendation. YK and YS provided some intellectual recommendation and reviewed the manuscript. CMI. conceived of the study, and participated in its design and coordination. All authors read and approved the final manuscript.

Competing interests

All authors declare there were no actual or potential conflicts of interest in this study.

Received: 17 October 2010 Accepted: 20 January 2011
Published: 20 January 2011

References

1. Barth RF, Coderre JA, Vicente MG, Blue TE: **Boron neutron capture therapy of cancer: current status and future prospects.** *Clin Cancer Res* 2005, **11**:3987-4002.
2. Yamamoto T, Nakai K, Matsumura A: **Boron neutron capture therapy for glioblastoma.** *Cancer Lett* 2008, **262**:143-52.
3. Pinelli T, Zonta A: **From the first idea to the application to the human liver.** Research and development in Neutron Capture Therapy; 2002.
4. Suzuki M, Sakurai Y, Hagiwara S, Masunaga S, Kinashi Y, Nagata K, Maruhashi A, Kudo M, Ono K: **First attempt of boron neutron capture therapy (BNCT) for hepatocellular carcinoma.** *Jpn J Clin Oncol* 2007, **37**:376-81.
5. Wittig A, Malago M, Collette L, Huiskamp R, Buhrmann S, Nievaart V, Kaiser G, Jockel KH, Sauerwein W: **BNCT in liver metastases: results of the EORTC trial 11001.** *Strahlentherapie Und Onkologie* 2007, **183**:115-115.
6. Sauerwein W, Malago M, Moss R, Altieri S, Hampel G, Wittig A, Nievaart V, Collette L, Mauri P, Huiskamp R, Michel J, Daquino G, Gerken G, Bornfeld N, Broelsch CE: **Boron Neutron Capture Therapy (BNCT) for the treatment of**

diffuse, non-resectable liver metastases. *Strahlentherapie Und Onkologie* 2006, **182**:109-109.

7. Cardose JE, Trivillin VA, Heber EM, Nigg DW, Calzetta O, Blaumann H, Longhino J, Itoiz ME, Bumaschny E, Pozzi E, Schwint AE: **Effect of Boron Neutron Capture Therapy (BNCT) on normal liver regeneration: Towards a novel therapy for liver metastases.** *International Journal of Radiation Biology* 2007, **83**:699-706.
8. Chou FI, Chung HP, Liu HM, Chi CW, Lui WY: **Suitability of boron carriers for BNCT: Accumulation of boron in malignant and normal liver cells after treatment with BPA, BSH and BA.** *Applied Radiation and Isotopes* 2009, **67**:105-108.
9. Wittig A, Malago M, Collette L, Huiskamp R, Buhrmann S, Nievaart V, Kaiser GM, Jockel KH, Schmid KW, Ortmann U, Sauerwein WA: **Uptake of two ^{10}B-compounds in liver metastases of colorectal adenocarcinoma for extracorporeal irradiation with boron neutron capture therapy (EORTC Trial 11001).** *Int J Cancer* 2008, **122**:1164-71.
10. Suzuki M, Masunaga SI, Kinashi Y, Takagaki M, Sakurai Y, Kobayashi T, Ono K: **The effects of boron neutron capture therapy on liver tumors and normal hepatocytes in mice.** *Jpn J Cancer Res* 2000, **91**:1058-64.
11. Sakurai Y, Ono K, Miyatake S, Maruhashi A: **Improvement effect on the depth-dose distribution by CSF drainage and air infusion of a tumour-removed cavity in boron neutron capture therapy for malignant brain tumours.** *Phys Med Biol* 2006, **51**:1173-83.
12. Wu G, Barth RF, Yang W, Lee RJ, Tjarks W, Backer MV, Backer JM: **Boron containing macromolecules and nanovehicles as delivery agents for neutron capture therapy.** *Anticancer Agents Med Chem* 2006, **6**:167-84.
13. Mehta SC, Lu DR: **Targeted drug delivery for boron neutron capture therapy.** *Pharm Res* 1996, **13**:344-51.
14. Maruyama K, Ishida O, Kasaoka S, Takizawa T, Utoguchi N, Shinohara A, Chiba M, Kobayashi H, Eriguchi M, Yanagie H: **Intracellular targeting of sodium mercaptoundecahydrododecaborate (BSH) to solid tumors by transferrin-PEG liposomes, for boron neutron-capture therapy (BNCT).** *J Control Release* 2004, **98**:195-207.
15. Masunaga S, Kasaoka S, Maruyama K, Nigg D, Sakurai Y, Nagata K, Suzuki M, Kinashi Y, Maruhashi A, Ono K: **The potential of transferrin-pendant-type polyethyleneglycol liposomes encapsulating decahydrodecaborate-(^{10})B (GB-10) as (^{10})B-carriers for boron neutron capture therapy.** *Int J Radiat Oncol Biol Phys* 2006, **66**:1515-22.
16. Doi A, Kawabata S, Iida K, Yokoyama K, Kajimoto Y, Kuroiwa T, Shirakawa T, Kirihata M, Kasaoka S, Maruyama K, Kumada H, Sakurai Y, Masunaga S, Ono K, Miyatake S: **Tumor-specific targeting of sodium borocaptate (BSH) to malignant glioma by transferrin-PEG liposomes: a modality for boron neutron capture therapy.** *J Neurooncol* 2008, **87**:287-94.
17. Aljabri MR, Lodato F, Burroughs AK: **Surveillance and diagnosis for hepatocellular carcinoma.** *Liver Transpl* 2007, **13(11 Suppl 2)**:S2-12.
18. World Health Organization: **World Health Statistics 2008/Future trends in global mortality.**[http://www.who.int/whosis/whostat/2008/en/index.html].
19. Arciero CA, Sigurdson ER: **Diagnosis and treatment of metastatic disease to the liver.** *Semin Oncol* 2008, **35**:147-59.
20. Kaneda Y, Nakajima T, Nishikawa T, Yamamoto S, Ikegami H, Suzuki N, Nakamura H, Morishita R, Kotani H: **Hemagglutinating virus of Japan (HVJ) envelope vector as a versatile gene delivery system.** *Mol Ther* 2002, **6**:219-26.
21. Mima H, Yamamoto S, Ito M, Tomoshige R, Tabata Y, Tamai K, Kaneda Y: **Targeted chemotherapy against intraperitoneally disseminated colon carcinoma using a cationized gelatin-conjugated HVJ envelope vector.** *Mol Cancer Ther* 2006, **5**:1021-8.
22. Kawano H, Komaba S, Kanamori T, Kaneda Y: **A new therapy for highly effective tumor eradication using HVJ-E combined with chemotherapy.** *BMC Med* 2007, **5**:1-7.
23. Kurooka M, Kaneda Y: **Inactivated Sendai virus particles eradicate tumors by inducing immune responses through blocking regulatory T cells.** *Cancer Res* 2007, **67**:227-36.
24. Fujihara A, Kurooka M, Miki T, Kaneda Y: **Intratumoral injection of inactivated Sendai virus particles elicits strong antitumor activity by enhancing local CXCL10 expression and systemic NK cell activation.** *Cancer Immunol Immunother* 2008, **57**:73-84.
25. Mima H, Tomoshige R, Kanamori T, Tabata Y, Yamamoto S, Ito S, Tamai K, Kaneda Y: **Biocompatible polymer enhances the in vitro and in vivo transfection efficiency of HVJ envelope vector.** *J Gene Med* 2005, **7**:889-97.
26. Asai T, Ueda T, Itoh K, Yoshioka K, Aoki Y, Mori S, Yoshikawa H: **Establishment and characterization of a murine osteosarcoma cell line (LM8) with high metastatic potential to the lung.** *Int J Cancer* 1998, **76**:418-422.
27. Lee CM, Tanaka T, Murai T, Kondo M, Kimura J, Su W, Kitagawa T, Ito T, Matsuda H, Miyasaka M: **Novel chondroitin sulfate-binding cationic liposomes loaded with cisplatin efficiently suppress the local growth and liver metastasis of tumor cells in vivo.** *Cancer Res* 2002, **62**:4282-8.
28. Fukunaka Y, Iwanaga K, Morimoto K, Kakemi M, Tabata Y: **Controlled release of plasmid DNA from cationized gelatin hydrogels based on hydrogel degradation.** *J Control Release* 2002, **80**:333-43.
29. Hosseinkhani H, Aoyama T, Ogawa O, Tabata Y: **Ultrasound enhancement of in vitro transfection of plasmid DNA by a cationized gelatin.** *J Drug Target* 2002, **10**:193-204.
30. Nagata I, Kimura Y, Ito Y, Tanaka T: **Temperature-Sensitive Phenomenon of Viral Maturation Observed in BHK Cells Persistently Infected with HVJ.** *Virology* 1972, **49**:453-461.
31. Guttenberger M: **Protein Determination.** *Cell Biology A Laboratory Handbook*:295-303.
32. Ogura K, Yanagie H, Eriguchi M, Lehmann EH, Kuhne G, Bayon G, Kobayashi H: **Neutron capture autoradiographic study of the biodistribution of ^{10}B in tumor-bearing mice.** *Appl Radiat Isot* 2004, **61**:585-90.
33. Saga K, Tamai K, Kawachi M, Shimbo T, Fujita H, Yamazaki T, Kaneda Y: **Functional modification of Sendai virus by siRNA.** *J Biotechnol* 2008, **133**:386-94.
34. Maeda H, Wu J, Sawa T, Matsumura Y, Hori K: **Tumor vascular permeability and the EPR effect in macromolecular therapeutics: a review.** *J Control Release* 2000, **65**:271-84.
35. Siwak DR, Tari AM, Lopez-Berestein G: **The potential of drug-carrying immunoliposomes as anticancer agents. Commentary re: J. W. Park et al., Anti-HER2 immunoliposomes: enhanced efficacy due to targeted delivery.** *Clin Cancer Res* 2002, **8**:1172-1181, Clin Cancer Res 2002,8:955-6.
36. Yanagie H: **Selective Enhancement of Boron Accumulation with Boron-Entrapped Water-in-oil-in-water Emulsion in VX-2 Rabbit Hepatic Cancer Model for BNCT.** Proc of 12th International Congress of Neutron Capture Therapy; 2006.
37. Ye SJ: **Monte Carlo based protocol for cell survival and tumour control probability in BNCT.** *Phys Med Biol* 1999, **44**:447-61.
38. Kobayashi T, Kanda K: **Analytical calculation of boron- 10 dosage in cell nucleus for neutron capture therapy.** *Radiat Res* 1982, **91**:77-94.
39. Kinashi Y, Masunaga S, Nagata K, Suzuki M, S T, Ono K: **A bystander effect observed in boron neutron capture therapy: A study of the induction of mutations in the HPRT locus.** *Int J Radiat Oncol Biol Phys* 2007, **68**:508-14.
40. Suzuki M, Sakurai Y, Masunaga S, Kinashi Y, Nagata K, Ono K: **Dosimetric study of boron neutron capture therapy with borocaptate sodium (BSH)/lipiodol emulsion (BSH/lipiodol-BNCT) for treatment of multiple liver tumors.** *Int J Radiat Oncol Biol Phys* 2004, **58**:892-6.
41. Suzuki M, Nagata K, Masunaga S, Kinashi Y, Sakurai Y, Maruhashi A, Ono K: **Biodistribution of ^{10}B in a rat liver tumor model following intra-arterial administration of sodium borocaptate (BSH)/degradable starch microspheres (DSM) emulsion.** *Appl Radiat Isot* 2004, **61**:933-7.
42. Yanagie H, Tomita T, Kobayashi H, Fujii Y, Nonaka Y, Saegusa Y, Hasumi K, Eriguchi M, Kobayashi T, Ono K: **Inhibition of human pancreatic cancer growth in nude mice by boron neutron capture therapy.** *Br J Cancer* 1997, **75**:660-5.
43. Yanagie H, Sakurai Y, Ogura K, Kobayashi T, Furuya Y, Sugiyama H, Kobayashi H, Ono K, Nakagawa K, Takahashi H, Nakazawa M, Eriguchi M: **Evaluation of neutron dosimetry on pancreatic cancer phantom model for application of intraoperative boron neutron-capture therapy.** *Biomed Pharmacother* 2007, **61**:505-14.
44. Suzuki M, Sakurai Y, Masunaga S, Kinashi Y, Nagata K, Maruhashi A, Ono K: **A preliminary experimental study of boron neutron capture therapy for malignant tumors spreading in thoracic cavity.** *Jpn J Clin Oncol* 2007, **37**:245-9.
45. Kawano H, Komaba S, Yamasaki T, Maeda M, Kimura Y, Maeda A, Kaneda Y: **New potential therapy for orthotopic bladder carcinoma by combining HVJ envelope with doxorubicin.** *Cancer Chemother Pharmacol* 2008, **61**:973-8.

doi:10.1186/1748-717X-6-8
Cite this article as: Fujii *et al.*: Cationized gelatin-HVJ envelope with sodium borocaptate improved the BNCT efficacy for liver tumors *in vivo*. *Radiation Oncology* 2011 **6**:8.

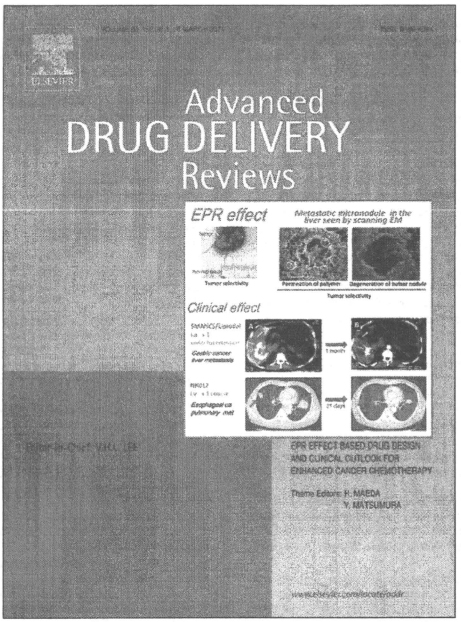

Advanced Drug Delivery Reviews 63 (2011) 161–169

Contents lists available at ScienceDirect

Advanced Drug Delivery Reviews

journal homepage: www.elsevier.com/locate/addr

Intracellular targeting delivery of liposomal drugs to solid tumors based on EPR effects☆

Kazuo Maruyama *

Faculty of Pharmaceutical Sciences, Teikyo University, 1091-1, Suarashi, Midori-ku, Sagamihara, 252-5195 Japan

ARTICLE INFO

Article history:
Received 18 March 2010
Accepted 1 September 2010
Available online 28 October 2010

Keywords:
Liposome
PEG-liposome
Transferrin
Boron neutron-capture therapy (BNCT)
Oxaliplatin
Passive targeting
Intracellular targeting
Fab' fragment

ABSTRACT

The success of an effective drug delivery system using liposomes for solid tumor targeting based on EPR effects is highly dependent on both size ranging from 100-200 nm in diameter and prolonged circulation half-life in the blood. A major development was the synthesis of PEG-liposomes with a prolonged circulation time in the blood. Active targeting of immunoliposomes to the solid tumor tissue can be achieved by the Fab' fragment which is better than whole IgG in terms of designing PEG-immunoliposomes with prolonged circulation. For intracellular targeting delivery to solid tumors based on EPR effects, transferrin-PEG-liposomes can stay in blood circulation for a long time and extravasate into the extravascular of tumor tissue by the EPR effect as PEG-liposomes. The extravasated transferrin-PEG-liposomes can maintain anti cancer drugs in interstitial space for a longer period, and deliver them into the cytoplasm of tumor cells via transferrin receptor-mediated endocytosis. Transferrin-PEG-liposomes improve the safety and efficacy of anti cancer drug by both passive targeting by prolonged circulation and active targeting by transferrin.

Contents

1. Introduction

It was the German bacteriologist Paul Ehrlich who, in the late nineteenth century, coined the term "magic bullet", meaning a chemical that travels through the body and selectively kills diseased cells without harming neighboring healthy cells. Since then, many different approaches based on various physical and biochemical principles have been examined with the goal of developing systems with a therapeutically acceptable degree of target specificity. Understanding target structure and function, developing drug delivery strategies to achieve controlled release, and targeting of drugs to specific tissues of the body, have been a major focus of research in an attempt to improve selectivity in cancer treatment. Currently, the concept of the "magic bullet" includes a coordinated behavior of three components: (A) drug; (B) targeting moiety; and (C) pharmaceutical carrier. Pharmaceutical carriers include soluble polymers, microcapsules, microparticles, cells, cell ghosts, proteins including monoclonal antibody, lipoproteins, micelles, and liposomes.

The use of liposomes in drug delivery as the "magic bullet" has been extensively studied (for recent books, see ref. [1,2]). Liposomal carriers have a strong impact on pharmacokinetics and on the tissue distribution of incorporated drugs. The pharmacokinetic parameters

☆ This review is part of the *Advanced Drug Delivery Reviews* theme issue on "EPR effect based drug design and clinical outlook for enhanced cancer chemotherapy".

* Corresponding author. Tel.: +81 42 685 3722; fax: +81 42 685 3432.
E-mail address: maruyama@pharm.teikyo-u.ac.jp.

0169-409X/$ – see front matter © 2010 Elsevier B.V. All rights reserved.
doi:10.1016/j.addr.2010.09.003

of liposomes depend on the physicochemical characteristics of the liposomes, such as size, surface charge, membrane lipid packing, steric stabilization, dose, and route of administration [3,4]. These factors may lead to enhanced efficacy as well as reduced toxic side effects of antitumor drugs. Clinical trials have demonstrated a reduced risk of cardiotoxicity of normal and pegylated liposomal doxorubicin including compared to the free drug, while preserving antitumor activity [5]. However, a major drawback of liposomes is their rapid uptake and accumulation by phagocytic cells of the mononuclear phagocyte system (reticuloendothelial system (RES)) after systemic administration [6]. Conventional liposomes are opsonized by plasma proteins, quickly recognized as foreign bodies, and rapidly captured by the RES. The major organs of accumulation are the liver and the spleen due to their rich blood supply and the abundance of tissue-resident phagocytic cells. Such unwanted macrophage uptake during chemotherapy can be problematic since it may lead to partial depletion of macrophages and interfere with important host-defense functions of this cell type [7]. Depending on the size and composition of the liposome, RES uptake can occur within minutes after administration and remove the liposomes from the circulation. A liposome with a diameter larger than 400 nm cannot circulate in the blood stream for long since it is quickly captured by the RES, whereas a liposome with a diameter<200 nm can remain in circulation for a long time [8,9].

The blood vessels in most normal tissues are non-fenestrated capillaries. These blood vessels are composed of a single layer of endothelial cells with tight junctions. In contrast, tumor blood vessels are inherently leaky, due to wide inter-endothelial junctions, the large number of fenestrae and transendothelial channels formed by vesicles, and a discontinuous or absent basement membrane [10,11]. Generally, the capillary permeability of the endothelial barrier in newly vascularized tumors is significantly greater than that of normal tissues [12].

The extravasation of liposomes from blood vessels to the tumor region is a function of both local blood flow and microvascular permeability [12]. Liposomes of the appropriate size can accumulate relatively easily into well-vascularized tumors through vascular fenestrations. However, it may take a long time for the liposome to reach an effective or maximum drug concentration level in the tumor or target site. In addition, due to little or no lymphatic drainage in tumor tissues, liposomes are, upon accumulation, retained in the tumor interstitium for a prolonged period. This phenomenon, termed the enhanced permeability and retention (EPR) effect, has been shown to occur universally among tumor types [13,14]. Therefore, the success of an effective drug delivery system using liposomes for tumor targeting based on EPR effects is highly dependent on prolonged circulation in the blood.

2. Passive targeting of the liposomal carrier to solid tumors based on EPR effects

To reach a target solid tumor site, liposomes must find the fenestrate (opening) on the tumor blood vessels through conventional flow and random diffusional processes. These processes, which are linked to probability issues, are called "passive targeting" coupled with "enhanced permeability". A major development in the last decade of the twentieth century was the synthesis of PEGylated liposomes (PEG-liposomes) with a prolonged circulation time in the blood. These liposomes are commonly called "stealth" liposomes, long-circulating liposomes, or sterically stabilized liposomes. PEG-liposomes containing polyethylene glycol derivatives of phosphatidyl ethanolamine (PEG-lipid) are not readily taken up by macrophages in the RES, and hence remain in the circulation for a relatively long period [15–18]. Normally, plasma proteins are easily adsorbed onto conventional liposome surfaces, easily caught by the RES, and eliminated from the body [9,19]. To avoid this rapid clearance, a hydrophilic compound is coated on the surface of the liposomes [15,20,21]. When PEG-lipid is inserted into liposomal membranes, an aqueous layer is formed by the localization of the PEG tether on the surface and adheres to the liposomes [22]. This modification prevents the recognition of the liposomes by opsonins (i.e., antibodies or components of the complement system) and therefore reduces their clearance by cells of the RES [23]. PEG-liposomes can remain in the blood circulation for extended periods (i.e., $t_{1/2}$>40 h) and distribute through an organism relatively evenly. Most of the liposomes distribute in the central compartment (i.e., the blood), with only 10% to 15% of the dose being delivered to the liver. This is a significant improvement over conventional liposomes where typically 80% to 90% of the liposomes deposit in the liver.

The extravasation of different-sized PEG-liposomes into solid tumors was examined in various tumor models in mice [24 and unpublished data]. As shown in Fig. 1 (left), long-circulating liposomes composed of DSPC/Chol/DSPE-PEG2000 (1:1:0.13, m/m) with an average diameter of 100-200 nm were accumulated efficiently in all tumor tissues examined. Liposome size was clearly another important factor for extravasation. Observations using fluorescence microscopy have shown that PEG-liposomes can indeed extravasate beyond the endothelial barrier mainly in postcapillary venules [25,26]. Extravasation and localization of PEG-liposomes were also examined by electron microscopy in Colon 26 tumor-bearing mice. As shown in Fig. 1 (right), wide inter-endothelial junctions were observed in tumor sections containing blood vessels. PEG-liposomes escaped from the gaps between adjacent endothelial cells and extensively penetrated into the extravascular and interstitial space among tumor cells. The size of the gaps between the cells that line tumor blood vessels has been estimated to be 100-600 nm [27], that is sufficiently large to allow the extravasation of small PEG-liposomes from the vessel to tumor interstitial space. Due to the increased circulation time of liposomes containing PEG-lipid and the leaky structure of microvasculature in the solid tumor tissue, these liposomes have been shown to accumulate preferentially in tumor tissue. Thus, under physiological tumor conditions, only small liposomes ranging from 100-200 nm in diameter with a prolonged circulation half-life have a significant chance of encountering the leaky vessels of tumor tissue.

3. Clinical development of liposomal anti-cancer drugs based on EPR effects

Base on the EPR effect, many liposomal drugs for passive targeting are being developed as a new class of antitumor agents [28–30]. At present, several liposomal anticancer drugs are available in the clinic or are in advanced stages of clinical development, as shown in Table 1. Clinical studies have shown that conventional liposomes are taken up by liver macrophages and destroyed with a half-life in body fluids of 20 min [31]. On the contrary, PEG-liposomes display a half-life of 5 days in these body fluids [32]. Liposomal drug formulations offer the possibility of increasing efficacy while reducing the toxic side effects of cytotoxic chemotherapeutic drugs.

The clinical use of liposomal formulations of conventional cytostatic drugs focused initially on anthracyclines, since these cationic amphiphiles allow efficient and stable liposomal entrapment. Liposomal formulations of anthracyclines are used for the treatment of ovarian and breast cancer, and of HIV associated Kaposi's sarcoma. Anthracyclines bear a high risk of causing acute and cumulative cardiotoxicity (resulting in cardiomyopathy), which limits their use. Liposomal formulations can solve these problems [28,33] since the altered pharmacokinetics of liposomal anthracyclines offers the possibility of avoiding high plasma peaks owing to drug retention within the liposomal formulation.

There are very interesting summarized data by Huwyler et al. [34] that compare the pharmacokinetic properties in human of Doxil/

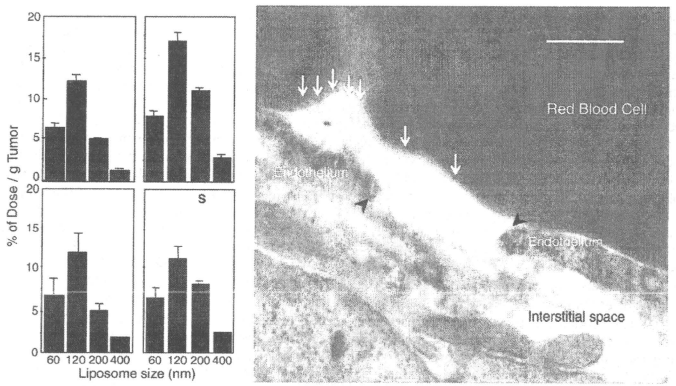

Fig. 1. *Left:* Effect of liposome size on the extravasation of PEG-liposomes into tumor tissue. Liposomes were injected into tumor-bearing mice via the tail vein and biodistribution was investigated at 6 h after injection. Tumor-bearing mice were prepared by inoculating tumor cells ($\sim 1 \times 10^7$) s.c. and were tested when the tumor mass volume reached about 1000-1500 mm^3. *Right:* Electron micrographs showing extravasation and localization of PEG-liposomes (126 ± 35 nm mean diameter) in Colon 26 solid tumor tissue. Liposomes were injected into mice via the tail vein, and the ultrathin sections of tumor tissue were prepared at 24 hr after administration. Between arrowheads : the gap between adjacent endothelial cells, Arrows : liposomes across the gap. Bar = 500 nm.

Caelyx (PEG-liposomal formulation), Myocet (conventional liposomal formulation) and free doxorubicin. Data from representative studies of Hamilton et al. [35], Gabizon et al. [36] and Mross et al. [37], were normalized using an average body surface area of 1.7 m^2 and an average body weight of 70 kg. As shown in Table 2, there are significant differences between the different formulation principles. Doxil/Caelyx shows minimal interaction with non-diseased tissues, leading to both a low systemic plasma clearance as well as a low volume of distribution of 0.03–0.05 L/kg. Consequently, Doxil/Caelyx shows a significantly lower risk of cardiotoxicity [38]. A reduced distribution of liposomal anthracyclines to heart muscle is observed using PEG-liposomes. This site avoidance of a drug-sensitive tissue is paralleled by enhanced drug deposition in tumor tissue (passive tumor targeting) leading to a pharmacodynamic advantage compared to the free drug [39]. Thus, the improved therapeutic index arises from both enhanced efficacy and reduced toxicity.

4. Active targeting of the liposomal carrier to solid tumor

Passive targeting of liposomal drugs to the solid tumor tissue can be achieved by the so called EPR effect. Their specificity can be markedly enhanced when tumor targeting ligands are used. Among the various approaches to active targeting, immunoliposomes using an antibody as a targeting ligand and a lipid vesicle as a carrier for both hydrophobic and hydrophilic drugs have attracted much attention [40,41]. Studies have revealed *in vivo* that coating liposomes with antibody leads to enhanced uptake of the immunoliposomes by the RES [42,43], and the immuno-targeting efficiency depends on the antibody density on the surface [44]. Thus, highly efficient targeting and a relatively low level of RES uptake of immunoliposomes are apparently mutually exclusive.

To study whether immunoliposomes injected intravenously can extravasate into solid tumors and bind to tumor cells, we used the monoclonal antibody 21B2, specific for the human carcinoembryonic antigen (CEA), and mice bearing CEA-positive human gastric cancer strain MKN-45 [45]. 21B2 was isolated from BALB/c mice after immunization with human CEA antigen, purified from CEA-producing human gastric cancer strain MKN-45 cells. Fab' fragments of 21B2 were prepared by pepsin digestion of the antibody and 2-aminoethanethiol reduction of the $F(ab')_2$ fragments. A series of PEG-immunoliposomes were designed to investigate the role of PEG molecules in immunoliposome binding to the target cells. We synthesized distearoyl-N-(3-carboxypropionoyl) polyethyleneglycol phosphatidylethanolamine (DSPE-PEG-COOH), and the dipalmitoyl phosphatidyl ethanolamine derivative of PEG (DPPE-PEG), for the preparation of IgG-PEG-immunoliposomes and Fab'-PEG-immunoliposomes, respectively [46,47]. In *in vitro* binding assays, PEG-immunoliposomes conjugated with either IgG (whole antibody of 21B2) or the Fab' fragment of 21B2 readily bound to MKN-45 cells. These results revealed that free PEG (not linked to the antibody) in

Table 1
Liposomal drugs on the market.

Formulation	Drug	Product	Seller
Conventional liposome	Doxorubicin	Myocet	Elan
	Daunorubicin	DaunoXome	Gilead
	Cytarabine	DepoCyte	Skye Pharma/Enzon/ Mundipharma
	Vincristine	Marqibo	Hana Biosciences
PEG-liposome	Doxorubicin	Doxil/Caelyx	Alza/J&J/Schering-Plough
	Cisplatin	Lipoplatin	Regulon
	Belotecan	Camtobell(CK D602)	Alza/J&J

Table 2
Pharmacokinetic properties in human of free doxorubicin, conventional liposomal doxorubicin (Myocet) and PEG-liposomal doxorubicin (Doxil, Caelyx). Liposome diameter: 85 to 150 nm. Data normalisation using an average body surface area of 1.7 m^2 and an average body weight of 70 kg. Examples of representative studies: Hamilton et al., 2002; Gabizon et al., 2003; Mross et al. 2004.

	Free doxorubicin	Myocet conventional liposomal	Doxil/Caelyx PEG-liposome
Dose (mg/kg)	1.2	1.8	1.5
AUC (mg.h/L)	3.5	19.4	4082
Clearance (ml/h)	25300	9520	23
Vss (L)	365	139	3.0
Half-life (h)	0.06/10.4*	<1/52.6*	84

*Two elimination phases.

liposomes does not interfere sterically with antigen binding of the antibody or Fab' fragment.

The tissue distribution of IgG-PEG-immunoliposomes and Fab'-PEG-immunoliposomes was examined by inoculating CEA-positive human gastric cancer strain MKN-45 cells inoculated into BALB/c *nu/nu* mice. As shown in Fig. 2, PEG-Mal liposomes without the antibody showed prolonged residence in the circulation and low liver uptake, regardless of the presence of the terminal maleimidyl group. There were no marked differences in tissue distribution among liposomes containing DSPE-PEG(-OCH_3), DSPE-PEG-COOH and DPPE-PEG-Mal. IgG-PEG-immunoliposomes, bearing approximately 51 molecules of 21B2 (whole antibody) per liposome, were rapidly cleared from the blood and were found entirely in the liver. In contrast, Fab'-PEG-immunoliposomes, bearing approximately 517 Fab' molecules of 21B2 per liposome, were retained longer in the circulation, with a concomitant decrease in the liver uptake compared with IgG-PEG-immunoliposomes. These results indicate that the linkage of whole 21B2 antibodies to the PEG termini enhances RES uptake via the Fc receptor-mediated mechanism [42,43]. To overcome this problem, it is necessary to use the Fab' fragment. In the case of Fab'-PEG-immunoliposomes, the absence of the Fc portion and the presence of free PEG-Mal (not linked to the Fab' fragment) may both play a role in prolonging the circulation of the liposomes. Thus, the Fab' fragment is much better than whole IgG in terms of designing PEG-immunoliposomes with prolonged circulation. Further, the usage of the Fab' fragment should greatly reduce the antigenicity.

We next investigated whether Fab'-PEG-immunoliposomes could extravasate into solid tumor tissue and bind to tumor cells. Fig. 2 shows the accumulation of Fab'-PEG-immunoliposomes, IgG-PEG-immunoliposomes and comparable PEG-liposomes, with an average diameter of 100–130 nm, in MKN-45 solid tumors 24 h after injection in mice. Relatively high accumulation was obtained with PEG-COOH liposomes, PEG-Mal liposomes and Fab'-PEG-immunoliposomes. These results were clearly correlated to their prolonged circulation time. The accumulation rate of Fab'-PEG-immunoliposomes was 2-fold higher than that of IgG-PEG-immunoliposomes or bare liposomes, and equal to that of PEG-Mal or PEG-COOH liposomes. The permeability of tumor vasculature is generally increased compared to normal tissue, so the smaller Fab'-PEG-immunoliposomes with its prolonged circulation time could extravasate through the leaky endothelium by passive convective transport. Ligand-directed targeting by Fab'-recognition is rather weak. On the other hand, IgG-PEG-immunoliposomes exhibited a short circulation time due to high liver uptake, so they lack both sufficient concentration and residence time to allow extravasation through the leaky endothelium. Though there were no differences in accumulation into solid tumors between Fab'-PEG-immunoliposomes and PEG-liposomes without antibodies, only Fab'-PEG-immunoliposomes stand a better chance of binding to the surface of MKN-45 cells. This is important for the extravasated Fab'-PEG-immunoliposomes, because Fab'-PEG-immunoliposomes can bind readily with MKN-45 cells in *in vitro* binding assays. This delivery system is particularly important for the endocytotic internalization of bioactive materials. However, in some other cases, the liposome internalization seems not to be important. It was shown in Sapra and Allen [48] that PEG-liposomes loaded with vincristin or doxorubicin and modified with antibodies against internalizing CD19 antigen or noninternalizing CD20 antigen demonstrate therapeutic effect which dependent more on the type of drugs used than on its ability to be internalized. The cytotoxicity of target liposomes depended also on the rate of drug release from the liposomes.

5. Liposomal drugs for intracellular targeting delivery to solid tumors based on EPR effects

Tumor-specific targeting therapies have been advocated as a means of increasing the therapeutic effect and decreasing the side effects of drugs. Intracellular targeting using iron-saturated transferrin (TF) as a ligand for receptor-mediated endocytosis has attracted attention. TF is a glycoprotein that transports ferric ions in the body, and TF receptor is internalized into cells by endocytosis through the binding of TF. This receptor-mediated endocytosis is a normal physiological process by which iron is delivered into cells [49,50].

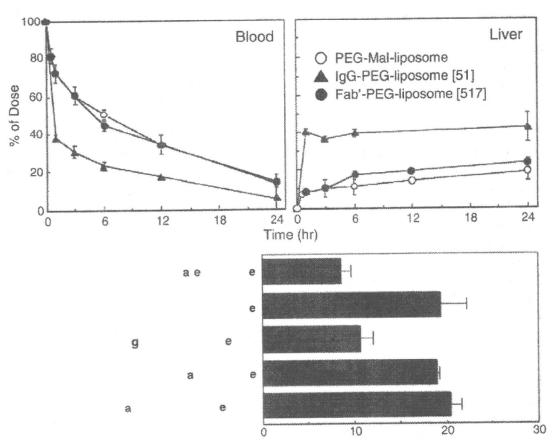

Fig. 2. Time course of blood residence, liver uptake and tumor accumulation of PEG-liposomes, IgG-PEG-liposome [51] or Fab'-PEG-liposome [517] in MKN-45- bearing BALB/c nu/nu mice. Two million MKN-45 cells were inoculated into the backs of female BALB/c nu/nu mice. The numbers in parentheses represent the average numbers of whole antibodies of 21B2 or Fab' molecules of 21B2 per liposome.

After binding of TF to the receptors on the cell surface, the TF-receptor complexes are internalized to form endosomes through clathrin-coated vesicles. After internalization, iron-loaded TF releases its iron due to the low endosomal pH, while iron-free TF remains bound to the receptor. These complexes are sorted into exocytic vesicles for delivery back to the cell surface and iron-free TF is released. The entire TF cycle takes only 4–5 min, with a mean transit time of about 10 min, and avoids the lysosomal compartment. As the TF receptor concentration on the cell membrane is reported to be higher in various types of tumor cells than in normal cells, correlating with the aggressive or proliferate ability of cells [50,51]. TF receptor is considered to be useful as a potential target for drug delivery into tumor cells.

We have explored the possibility of using TF for developing an intracellular drug delivery system [52]. TF was coupled to the distal termini of the PEG chains to prepare TF-PEG-liposome, as previously described [52]. TF-PEG-liposomes, bearing approximately 25 TF molecules per liposome, readily bound to mouse Colon 26 cells *in vitro*, and were internalized by receptor-mediated endocytosis.

TF-PEG-liposomes exhibited interesting properties with regards to biodistribution, tumor accumulation and internalization *in vivo*. As shown in Fig. 3, TF-PEG-liposomes had a prolonged circulation time and low RES uptake in Colon 26 tumor-bearing mice, resulting in enhanced extravasation of the liposomes into the solid tumor tissue. Coupling of TF molecules did not enhance RES uptake of liposomes, presumably because TF is an abundant serum glycoprotein (2.5 mg/ml) that transports ferric ion in the body. Electron microscopy studies in Colon 26 tumor-bearing mice revealed that the extravasated TF-PEG-liposomes were internalized into tumor cells by receptor-mediated endocytosis. TF-PEG-liposomes were taken up into endosomal-like intracellular vesicles, as visualized by transmission electron microscopy (data not shown) and maintained a high drug level in the tumor for over 60 h after injection (Figs. 3 and 4). This high retention indicates cellular uptake of the extravasated TF-PEG-liposomes by TF-receptor-mediated endocytosis. Thus, TF-PEG-liposomes are potential tools for *in vivo* cytosolic delivery of anticancer drugs in cancer chemotherapy, as well as of nucleic acids in gene therapy.

We and Liu et al. previously demonstrated that a relatively high level of tumor accumulation of PEG-liposomes correlated very well with both a small size (less than 200 nm in diameter) and a relatively high concentration of liposomes in the blood [9,25,52]. Though there were no marked differences in accumulation in solid tumors between TF-PEG-liposomes and PEG-liposomes averaging 120 nm in diameter, only TF-PEG-liposomes bound specifically to tumor cells. Notably, the residence time of extravasated TF-PEG-liposomes in tumor tissues was much longer than that of PEG-liposomes (Fig. 4). TF-PEG-liposomes escaped from leaky endothelial barriers and extravasated into the extravascular and interstitial space among tumor cells.

Huwyler et al. pointed out in their review [34] that the transferrin receptor (which has a dissociation constant of 5.6 nM) is saturated *in vivo* by the μM endogenous plasma transferrin concentrations [53]. This strong competition with endogenous transferrin leads to poor *in vivo* receptor targeting after intravenous injection. However, *in vivo* data (Figs. 3 and 4) of TF-PEG-liposomes showed that this strong competition tends to inhibit the binding of TF-PEG-liposomes to normal cells after intravenous injection. Consequently, TF-PEG-liposomes remain in blood circulation for a long period and extravasate into the extravascular of tumor tissue by the EPR effect as PEG-liposomes. The decreased flow in the interstitial space among tumor cells provides TF-PEG-liposomes with a greater chance to bind to the TF receptors on the surface of the tumor cells, even in the presence of endogenous plasma transferrin.

6. Intracellular targeting of sodium mercaptoundecahydrododecaborate (^{10}BSH) to solid tumors by transferrin-PEG liposomes, for boron neutron-capture therapy (BNCT) [54]

BNCT is aimed at inhibiting the growth of various cancers [55]. The stable isotope of boron, ^{10}B, interacts with low energy (thermal) neutrons to produce highly energetic, short-range disintegration products. The resultant lithium ions and particles are high linear energy transfer particles with relatively high biological efficiency. These particles (α and ^{7}Li) destroy cells within a radius about 10 μm from the site of the capture reaction. It is theoretically possible to kill tumor cells without affecting adjacent healthy cells if ^{10}B atoms can be selectively accumulated in the interstitial space of tumor tissue and/or the intracellular space between tumor cells. The neutron component of this therapy by itself would have little effect on tumor or normal tissue, and thermal neutrons (<0.4 eV) have insufficient energy to damage tissue. The preferential localization of a ^{10}B compound in a tumor cell, followed by neutron irradiation, results in the destruction of the tumor cell without damage to surrounding normal cells [56]. When ^{10}B is present on the cell surfaces of a tissue, its cell-killing effect is greatly reduced compared to when it is accumulated inside the cell. Thus, successful treatment of cancer by BNCT requires the selective delivery of relatively large amounts of ^{10}B compounds to malignant cells. The estimated boron concentration required for effective therapy is in the range of 20–30 μg ^{10}B per g of tissue [57]. At the same time, the boron concentration in the surrounding normal tissue should be kept low to minimize damage to the normal tissue.

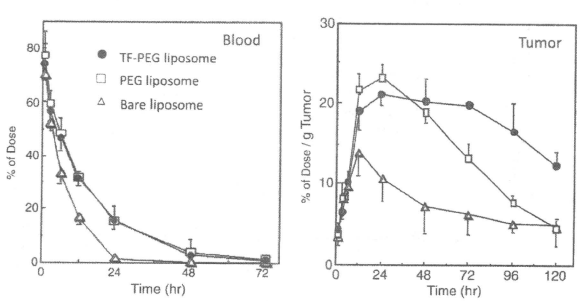

Fig. 3. Time courses of blood residence and tumor accumulation of TF-PEGliposomes, with an average of 25 TF molecules per liposome, after intravenous injection. Liposomes (100–130 nm average diameter) labeled with ^{3}H-CHE were injected into Colon 26 tumor-bearing mice at a dose of 500 μg lipid. Data are expressed as mean ± S.D. (n = 3–5).

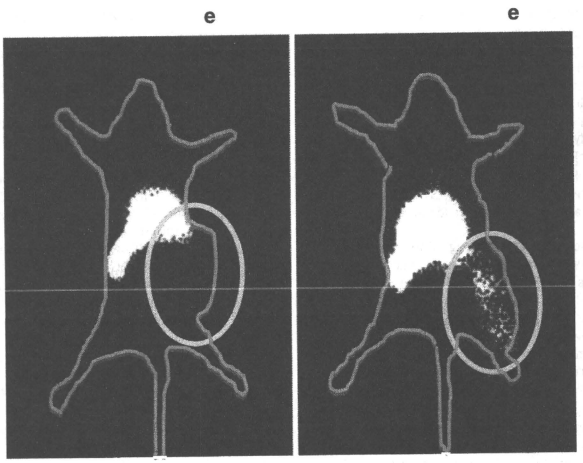

Fig. 4. Gamma ray imaging of TF-PEG liposome in Colon 26 solid tumor tissue *in vivo*. TF-PEG-liposomes of 132 ± 38 nm mean diameter, entrapping ^{111}In-DTPA and coupling an average of 25 TF molecules per liposome, were injected into mice *via* the tail vein, and gamma ray imaging were taken 60 hr after administration.

When TF-PEG liposomes with an average diameter of 100–200 nm were injected at a dose of 35 mg/kg ^{10}B, we observed prolonged circulation and low uptake by the RES in Colon 26 tumor-bearing mice, resulting in enhanced accumulation of ^{10}B into the solid tumor tissue (e.g., 35.5 μg/g) (Figs. 5 and 6). The most likely mechanism for this accumulation is the increased blood circulation time of liposomes and the leaky structure of the microvasculature in solid tumor tissue (the EPR effect). The accumulation of TF-PEG-liposomes and PEG-liposomes in tumor tissue is directly proportional to the AUC_{plasma} of the plasma clearance. TF-PEG liposomes produced high ^{10}B levels in the tumor, with concentrations over 30 μg/g for at least 72 h after injection. This high retention of ^{10}B in tumor tissue indicates that binding and concomitant cellular uptake of the extravasated TF-PEG liposomes occurs by TF receptor and receptor-mediated endocytosis, respectively. On the other hand, the level of ^{10}B in plasma decreased, resulting in a tumor/plasma ^{10}B ratio of 6.0 at 72 h after injection. Notably, the level of ^{10}B in plasma was very low at 72 h after injection of TF-PEG liposomes, from the viewpoint of preventing damage to the endothelium. Such damage can be serious if reactor exposures take place when plasma boron levels are high [32]. The long retention of TF-PEG liposomes in tumor tissue provides sufficient time for the plasma ^{10}B concentration to fall substantially, resulting in a tumor/plasma ratio of 6.0 at 72 h after injection. The level of ^{10}B in the liver was also low at this time. These characteristics are therapeutically favorable. Thus, ≥ 72 h after injection of TF-PEG liposomes was selected as a suitable time point for BNCT treatment.

Administration of BSH encapsulated in TF-PEG liposomes at a dose of 5 - 35 mg/kg ^{10}B and irradiation with 2×10^{12} neutrons/cm^2 for 37 min suppressed tumor growth and improved long-term survival compared with PEG liposomes, bare liposomes and free BSH. Thus, intravenous injection of TF-PEG liposomes can increase the tumor retention of ^{10}B atoms, which were introduced by receptor-mediated

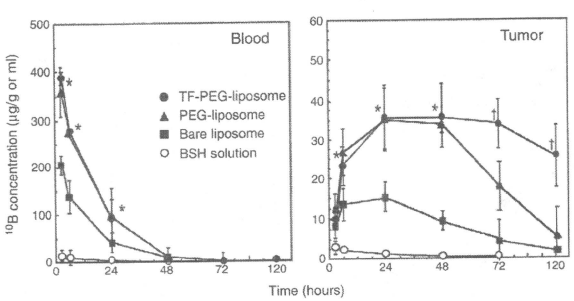

Fig. 5. Time courses of blood residence and tumor accumulation of ^{10}B delivered by each kind of liposome encapsulating BSH, and by BSH solution, in Colon 26 tumorbearing mice. Two hundred to 300 μl of BSH-TF-PEG liposomes, BSH-PEG liposomes, BSH bare liposomes or BSH solution was injected into tumor-bearing mice *via* the tail vein at a dose of 35 mg ^{10}B/kg. TF-PEG liposomes, with an average of 20 TF molecules per liposome, were used. Data are expressed as mean ± SD (n = 5).

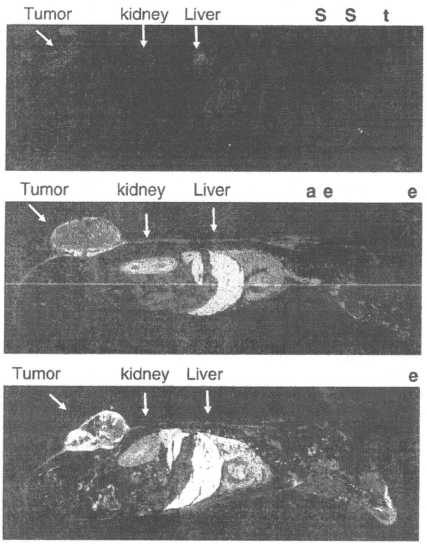

Fig. 6. Neutron capture autoradiography images of the wholebody section of Colon 26 bearing mice at 48 hr after iv injection.

endocytosis of liposomes after binding, causing tumor growth suppression *in vivo* upon thermal neutron irradiation. These results suggest that TF-PEG-liposomes are a suitable intracellular targeting carrier in BNCT therapy for cancer.

7. Intracellular targeting of oxaliplatin to solid tumors by transferrin-PEG liposomes

Oxaliplatin (trans-l-diaminocyclohexane oxalatoplatinum, L-OHP) is a novel cisplatin derivative that can reduce the side effects of cisplatin, such as toxicity to the kidneys. However, L-OHP is effective only when combined with 5-fluorouracil (5-FU) and leucovorin. The relatively low anti-tumor index of L-OHP alone is because only low levels accumulate in tumor tissues due to high partitioning to erythrocytes *in vivo*. A successful outcome of cancer therapy using L-OHP requires the selective delivery of a relatively high concentration of the drug to tumors.

We examined the tumor-selective delivery of L-OHP using TF-PEG-liposomes [58]. Fig. 7A shows the time course of plasma clearance after i.v. injection of L-OHP in solution and liposomal L-OHP. L-OHP in solution was rapidly cleared from the blood circulation whereas the circulation of L-OHP encapsulated within liposomes was increased. The blood concentrations of L-OHP encapsulated within PEG- and TF-PEG-liposomes were much higher than that of L-OHP encapsulated within Bare liposomes. Fig. 7B shows the biodistribution of L-OHP in solution and of L-OHP encapsulated within various liposomes at 6 h after intravenous (i.v.) injection. The results show that very little L-OHP was distributed to the major tissues in mice. In contrast, the distribution of L-OHP encapsulated in PEG- and TF-PEG-liposomes to the liver and spleen differed, but far less of both was distributed to these tissues compared with Bare liposomes. These results indicate that the PEG layer prolonged the systemic circulation of liposomes after i.v. injection. Thus, the conjugation of TF to the PEG termini did not alter the RES uptake of PEG-liposomes, presumably because TF is a blood glycoprotein.

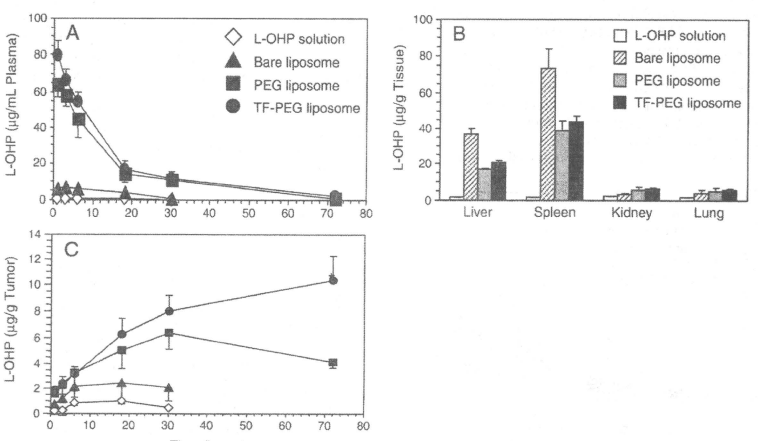

Fig. 7. Plasma clearance (A), biodistribution (B) and tumor accumulation of L-OHP solution or liposomal L-OHP in Colon 26-bearing mice. L-OHP in solution or encapsulated within Bare, PEG- or TF-PEG-liposomes (L-OHP: 5 mg/kg) was injected via tail veins of Colon 26-bearing mice. A: At various times thereafter, blood samples were collected using glass capillaries from veins of fundus oculi. Plasma L-OHP levels were measured by MIP-MS. B: Six hours later, mice were sacrificed and liver, spleen, kidneys and lungs were collected. C: At various times thereafter, tumor tissue was collected from the mice. Concentrations of L-OHP in tissue samples were measured by MIP-MS.

Fig. 7C shows the time course of L-OHP in Colon 26 solid tumor tissue after i.v. injection of L-OHP in solution or encapsulated within bare, PEG- or TF-PEG-liposomes. The concentrations of L-OHP in tumor tissue at 18 h after i.v. injection of L-OHP in solution and in bare liposomes were 0.98 and 2.1 μg/g tumor, respectively, and did not increase thereafter. The concentrations of L-OHP encapsulated within PEG- and TF-PEG-liposomes in tumor tissue were higher than that of L-OHP in solution and in bare liposomes. The L-OHP concentration in tumor tissue decreased 30 h after i.v. injection of L-OHP encapsulated within PEG-liposomes. Interestingly, the profiles of L-OHP encapsulated within TF-PEG- and PEG-liposomes in tumor tissues differed. The concentration of L-OHP encapsulated within TF-PEG-liposomes continued to increase until 72 h after i.v. injection, and a high L-OHP concentration was maintained in the tumor for a longer period. Tumor growth was somewhat suppressed to a similar extent by L-OHP in solution and encapsulated within bare or PEG-liposomes, but was significantly suppressed by L-OHP encapsulated within TF-PEG-liposomes (Fig. 8).

Effective anti-tumor therapy by L-OHP requires its internalization into the cytoplasm of tumor cells because this drug works by inhibiting DNA synthesis and transcription by forming DNA adducts [59]. The therapeutic effects of PEG-liposomes and L-OHP in solution were similar. It therefore appears that PEG-liposomes can deliver L-OHP to tumor tissue through the EPR effect, but are not effectively internalized into the cytoplasm. In contrast, TF-PEG-liposomes appear to deliver L-OHP into the cytoplasm of tumor cells via TF receptor-mediated endocytosis after extravasation by the EPR effect.

Actually, the retention time of PEG- and TF-PEG-liposomes in tumor tissues differed, despite their prolonged circulation in the blood. These results supported the notion that TF-PEG-liposomes deliver L-OHP to the surface and the interior of tumor cells. Prolonged circulation of TF-PEG-liposomes in the blood increased the amount of time that various tissues, including tumors, were exposed to L-OHP. In addition, TF receptors were also expressed on normal cells. We considered the possibility of a concomitant increase in the incidence of acute toxicity after a single L-OHP i.v. injection. However, blood biochemistry tests revealed that the tested parameters remained within their normal range. These findings indicated that L-OHP encapsulated within TF-PEG-liposomes did not induce any significant acute toxicity in the presence of increased distribution to the liver compared with L-OHP in solution. We also examined the biodistribution of L-OHP encapsulated within TF-PEG-liposomes in other experiments, and found that the concentration of L-OHP in the brain was very low (about 0.06 μg/g tissue) at 72 h after i.v. injection of the liposomes. Additionally, abnormal behavior was not observed in the mice. Therefore, it was thought that significant side effects were not induced in the brain. Furthermore, we did not observe any remarkable decrease in body weight after two i.v. injections of liposomal L-OHP. These results indicated that the frequency of serious side effects was minimal. Although L-OHP is a useful anti-tumor drug, it is rapidly cleared from the blood. We addressed this issue using TF-PEG-liposomes as a carrier for L-OHP. In conclusion, TF-PEG-liposomes, which allow both passive and active targeting, are a potential carrier for *in vivo* cytoplasmic targeting of L-OHP in solid tumors over-expressing surface TF receptors.

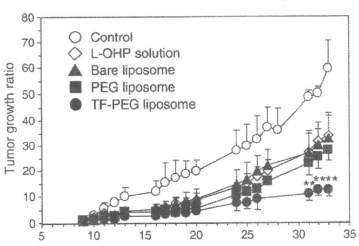

Fig. 8. Comparison of tumor growth suppression with L-OHP in solution and in liposomes in Colon 26-bearing mice. L-OHP solution or L-OHP encapsulated within Bare, PEG- or TF-PEG-liposomes (L-OHP: 5 mg/kg) was injected via tail veins of Colon 26-bearing mice on days 9 and 12 after tumor cell inoculation. Data are shown as means and standard deviation ($n=4$). $^{**}P<0.01$ (PEG-liposomes vs. TF-PEG-liposomes).

Based on the above results, MBP-426 was developed by a Japanese venture company. Phase I clinical trials for solid tumors are finished [60] and phase IIa studies are ongoing. MBP-426 is a transferrin-conjugated liposome formulation of oxaliplatin (L-OHP). MBP-426 improves the safety and efficacy of oxaliplatin by both passive targeting by prolonged circulation and active targeting by TF.

8. Conclusion

There are several clear aims when using ligand-mediated tumor targeting of drug-loaded nanocarriers compared to more traditional dosage forms [61]. Ideally, drugs in nanocarriers should not only accumulate in the interstitial space inside tumors but also be internalized by the target cells creating high intracellular drug concentration and allowing multidrug resistance to be bypassed. To achieve these goals, certain considerations should be taken into account: (1) a target should be identified which is present (over-expressed) on the surface of tumor cells in sufficient quantity providing good opportunity for the targeted liposomes to firmly bind with cancer cells; (2) the specific ligand should be attached to the surface of the drug-loaded nanocarriers in a way which does not affected its specific binding properties and long circulating activity in blood; (3) the targeting ligand is internalizable and facilitates the internalization of the carrier and carrier-incorporated anti-cancer drug; (4) drug release from carrier inside the tumor or inside the tumor cell should deliver the therapeutic concentration of the drug and maintain it for a reasonable period of time.

TF is a glycoprotein that transports ferric ions in the body, and TF receptor is internalized into cells by endocytosis through the binding of TF. TF-PEG-liposomes can stay in blood circulation for a long time and extravasate into the extravascular of tumor tissue by the EPR effect as PEG-liposomes. TF-PEG-liposomes can deliver incorporated anti-cancer drug into the cytoplasm of tumor cells via TF receptor-mediated endocytosis after extravasation by the EPR effect. Thus, TF-PEG-liposomes show promise in the clinical environment as a carrier for chemotherapy agents against various types of tumors that overexpress TF receptors.

References

[1] G. Gregoriadis, Liposome Technology, Third Ed.Informa, New York, 2007.
[2] V. Weissig, Liposomes, Springer, New York, 2009.
[3] D.C. Drummond, O. Meyer, K. Hong, D.B. Kirpotin, D. Papahadjopoulos, Optimizing liposomes for delivery of chemotherapeutic agents to solid tumors, Pharmacol. Rev. 51 (1999) 691–743.
[4] T.M. Allen, C. Hansen, Pharmacokinetics of stealth versus conventional liposomes: effect of dose, Biochim. Biophys. Acta 1068 (1991) 133–141.
[5] M.S. Ewer, F.J. Martin, C. Henderson, C.L. Shapiro, R.S. Benjamin, A.A. Gabizon, Cardiac safety of liposomal anthracyclines, Semin. Oncol. 31 (2004) 161–181.
[6] M.M. Frank, The reticuloendothelial system and bloodstream clearance, J. Lab. Clin. Med. 122 (1993) 487–488.
[7] T. Daemen, G. Hofstede, M.T. Ten Kate, I.A. Bakker-Woudenberg, G.L. Scherphof, Liposomal doxorubicin induced toxicity: depletion and impairment of phagocytic activity of liver macrophages, Int. J. Cancer 61 (1995) 716–721.
[8] K. Maruyama, T. Yuda, A. Okamoto, S. Kojima, A. Suginaka, M. Iwatsuru, Prolonged circulation time in vivo of large unilamellar liposomes composed of distearoyl phosphatidylcholine and cholesterol containing amphipathic poly(ethylene glycol), Biochim. Biophys. Acta 1128 (1992) 4–9.
[9] D. Liu, A. Mori, L. Huang, Role of liposome size and RES blockade in controlling biodistribution and tumor uptake of GM1-containing liposomes, Biochim. Biophys. Acta 1104 (1992) 95–101.

[10] R.K. Jain, Transport of molecules across tumor vasculature, Cancer Metastasis Rev. 6 (1987) 559.
[11] H.K. Dvorak, J.A. Nagy, J.T. Dvorak, A.M. Dvorak, Identification and characterization of the blood vessels of solid tumors that are leaky to circulating macromolecules, Am. J. Phathol. 133 (1988) 95–109.
[12] Y. Matsumura, H. Maeda, A new concept for macromolecular therapeutics in cancer chemotherapy: mechanism of tumoritropic accumulation of proteins and the antitumor agent smancs, Cancer Res. 46 (1986) 6387–6392.
[13] H. Maeda, The tumor blood vessel as an ideal target for macromolecular anticancer agents, J. Control. Release 19 (1992) 315–324.
[14] H. Maeda, L.W. Seymour, Y. Miyamoto, Conjugation of anticancer agents and polymers: advantages of macromolecular therapeutics in vivo, Bioconjug. Chem. 3 (1992) 351–362.
[15] A. Klibanov, K. Maruyama, V.P. Torchilin, L. Huang, Amphipathic polyethyleneglycols effectively prolong the circulation time of liposomes, FEBS Lett. 268 (1990) 235–237.
[16] G. Blume, C. Cevc, Liposomes for the sustained drug release in vivo, Biochim. Biophys. Acta 1029 (1990) 91–97.
[17] T.M. Allen, C. Hansen, F. Martin, C. Redemann, A.Y. Young, Liposomes containing synthetic lipid derivatives of poly(ethylene glycol) show prolonged circulation half-lives in vivo, Biochim. Biophys. Acta 1066 (1991) 29–36.
[18] K. Maruyama, T. Yuda, A. Okamoto, S. Kojima, A. Suginaka, M. Iwatsuru, Prolonged circulation time in vivo of large unilamellar liposomes composed of distearoyl phosphatidylcholine and cholesterol containing amphipathic poly(ethylene glycol), Biochim. Biophys. Acta 1128 (1992) 44–49.
[19] C. Allen, N. Dos Santos, R. Gallagher, G.N. Chiu, Y. Shu, W.M. Li, S.A. Johnstone, A.S. Janoff, L.D. Mayer, M.S. Webb, M.B. Bally, Controlling the physical behavior and biological performance of liposome formulations through use of surface grafted poly(ethylene glycol), Biosci. Rep. 22 (2002) 225–250.
[20] Y.S. Park, K. Maruyama, L. Huang, Some negatively charged phospholipid derivatives prolong the liposome circulation in vivo, Biochim. Biophys. Acta 1108 (1992) 257–260.
[21] K. Maruyama, S. Okuizumi, O. Ishida, H. Yamauchi, H. Kikuchi, M. Iwatsuru, Phosphatidyl polyglycerols prolong liposome circulation in vivo, Int. J. Pharm. 111 (1994) 103–107.
[22] Y. Sadzuka, A. Nakade, R. Hirama, A. Miyagishima, Y. Nozawa, S. Hirota, T. Sonobe, Effects of mixed polyethyleneglycol modification on fixed aqueous layer thickness and antitumor activity of doxorubicin containing liposome, Int. J. Pharm. 238 (2002) 171–180.
[23] S.M. Moghimi, H.M. Patel, Opsonophagocytosis of liposomes by peritoneal macrophages and bone marrow reticuloendothelial cells, Biochim. Biophys. Acta 1135 (1992) 269–274.
[24] S. Unezaki, K. Maruyama, O. Ishida, A. Suginaka, J. Hosoda, M. Iwatsuru, Enhanced tumor targeting and improved antitumor activity of doxorubicin by long-circulating liposomes containing amphipathic poly(ethylene glycol), Int. J. Pharm. 126 (1995) 41–48.
[25] S. Unezaki, K. Maruyama, J. Hosoda, I. Nagae, Y. Koyanagi, M. Nakata Test, article sample title placed here, Int. J. Pharm. 144 (1996) 11–17.
[26] S.K. Huang, K.D. Lee, K. Hong, D.S. Friend, D. Papahadjopoulos, Microscopic localization of sterically stabilized liposomes in colon carcinoma-bearing mice, Cancer Res. 52 (1992) 5135–5143.
[27] F. Yuan, M. Dellian, D. Fukumura, M. Leunig, D.A. Berk, V.P. Torchilin, R.K. Jain, Vascular permeability in a human tumor xenograft: molecular size dependence and cutoff size, Cancer Res. 55 (1995) 3752–3756.
[28] A.A. Gabizon, Pegylated liposomal doxorubicin: metamorphosis of an old drug into a new form of chemotherapy, Cancer Invest. 19 (2001) 424–436.
[29] J.W. Park, C.C. Benz, F.J. Martin, Future directions of liposomeand immunoliposome-based cancer therapeutics, Semin. Oncol. 31 (2004) 196–205.
[30] R.D. Hofheinz, S.U. Gnad-Vogt, U. Beyer, Liposomal encapsulated anti-cancer drugs, Anticancer Drugs 16 (2005) 691–707.
[31] F. Martin, T. Boulikas, The challenge of liposomes in gene therapy, Gene Ther. Mol. Biol. 1 (1998) 173–214.
[32] G.P. Stathopoulos, T. Boulikas, M. Vougiouka, G. Deliconstantinos, S. Rigatos, E. Darli, V. Viliotou, J.G. Stathopoulos, Pharmacokinetics and adverse reactions of a new liposomal cisplatin (Lipoplatin™): Phase I study, Oncol. Rep. 13 (2005) 589–595.
[33] D.N. Waterhouse, P.G. Tardi, L.D. Mayer, A comparison of liposomal formulations of doxorubicin with drug administered in free form: changing toxicity profiles, Drug Saf. 24 (2001) 903–920.
[34] J. Huwyler, J. Drewe, S. Krähenbuhl, Tumor targeting using liposomal antineoplastic drugs, Int. J. Nanomed. 3 (2008) 21–29.
[35] A. Hamilton, L. Biganzoli, R. Coleman, A phase I clinical and pharmacokinetic study of polyethylene glycol liposomal doxorubicin (Caelyx, Doxil) at a 6-week interval in patients with metastatic breast cancer, EORTC Ann. Oncol. 13 (2002) 910–918.
[36] A. Gabizon, H. Shmeeda, Y. Barenholz, Pharmacokinetics of pegylated liposomal Doxorubicin: review of animal and human studies, Clin. Pharmacokinet. 42 (2003) 419–436.
[37] K. Mross, B. Niemann, U. Massing, Pharmacokinetics of liposomal doxorubicin (TLC-D99; Myocet) in patients with solid tumors: an open-label, single-dose study, Cancer Chemother. Pharmacol. 54 (2004) 514–524.
[38] M.S. Ewer, F.J. Martin, C. Henderson, Cardiac safety of liposomal anthracyclines, Semin. Oncol. 31 (2004) 161–181.
[39] A.A. Gabizon, H. Shmeeda, S. Zalipsky, Pros and cons of the liposome platform in cancer drug targeting, J. Liposome Res. 16 (2006) 175–183.
[40] T.M. Allen, Liposomal Drug Formulations, Drugs 56 (1998) 747–756.
[41] K. Maruyama, O. Ishida, T. Takizawa, K. Moribe, Possibility of active targeting to tumor tissues with liposomes, Adv. Drug Deliv. Rev. 40 (1999) 89–102.
[42] D. Aragnol, L.D. Leserman, Immune clearance of liposomes inhibited by an anti-Fc receptor antibody in vivo, Proc. Natl Acad. Sci. USA 83 (1986) 2699–2703.
[43] J.T.P. Derksen, H.W.M. Marselt, G.L. Scherphof, Uptake and processing of immunoglobulin-coated liposomes by subpopulation of rat liver macrophages, Biochim. Biophys. Acta 971 (1988) 127–136.
[44] K. Maruyama, E. Holmberg, S.J. Kennel, A. Klibanov, V.P. Torchilin, L. Huang, Characterization of in vivo immunoliposome targeting to pulmonary endothelium, J. Pharm. Sci. 79 (1990) 978–984.
[45] I. Uyama, K. Kumai, T. Yasuda, T. Tagawa, K. Ishibiki, M. Kitajima, T. Tadakuma, Improvement of therapeutic effect by using Fab' fragment in the treatment of carcinoem bryonic antigen-positive human solid tumors with adriamycin-entrapped immunoliposomes, Jpn J. Cancer Res. 85 (1994) 434–440.
[46] K. Maruyama, T. Takizawa, T. Yuda, S.J. Kennel, L. Huang, M. Iwatsuru, Targetability of novel immunoliposomes modified with amphipathic polyethyleneglycols conjugated at their distal terminals to monoclonal antibodies, Biochim. Biophys. Acta 1234 (1995) 74–80.
[47] K. Maruyama, N. Takahashi, T. Tagawa, K. Nagaike, M. Iwatsuru, Immunoliposomes bearing polyethyleneglycol -coupled Fab' fragment show prolonged circulation time and high extravasation into target solid tumors in vivo, FEBS Lett. 413 (1997) 177–180.
[48] P. Sapra, T.M. Allen, Improved outcom when B-cell lymphoma is treated with combinations of immunoliposomal anticancer drugs targeted to both the CD19 and CD20 epitopes, Clin. Cancer Res. 10 (2004) 2530–2537.
[49] K. Thorstein, I. Romslo, The transferrin receptor: Its diagnostic value and its potential as therapeutic target, Scan. J. Clin. Lab. Invest. Suppl. 215 (1993) 113–120.
[50] E. Wagner, D. Curiel, M. Cotton, Delivery of drugs, proteins and genes into cells using transferrin as a ligand for receptor-mediated endocytosis, Adv. Drug Deliv. Rev. 14 (1994) 113–135.
[51] T. Miyamoto, N. Tanaka, Y. Eishi, T. Amagasa, Transferrin receptor in oral tumors, Int. J. Oral Maxillofac. Surg. 23 (1994) 430–433.
[52] O. Ishida, K. Maruyama, K. Sasaki, M. Iwatsuru, Size-dependent extravasation and interstitial localization of polyethyleneglycol liposomes in solid tumor-bearing mice, Int. J. Pharm. 190 (1999) 49–56.
[53] W.M. Pardridge, Brain drug delivery and blood-brain barrier transport, Drug Deliv. 1 (1993) 83–101.
[54] K. Maruyama, H. Yanagie, O. Ishida, S. Kasaoka, T. Takizawa, N. Utoguchi, A. Shinohara, M. Chiba, H. Kobayashi, M. Iwatsuru, M. Eriguchi, Intracellular targeting of sodium mercaptoundecahydrododecaborate (BSH) to solid tumors by transferrin-PEG liposomes, for boron neutron-capture therapy (BNCT), J. Control. Release 98 (2004) 195–207.
[55] M.F. Hawthorne, The role of chemistry in the development of boron neutron capture therapy of cancer, Angew. Chem. Int. Ed Engl. 32 (1993) 950–984.
[56] R.F. Barth, A.H. Soloway, R.G. Fairchild, Boron neutron capture therapy for cancer, Cancer Res. 50 (1990) 1061–1070.
[57] R.F. Barth, A.H. Soloway, R.G. Fairchild, R.M. Brugger, Boron neutron capture therapy for cancer. Cancer 70 (1992) 2995–3007.
[58] R. Suzuki, T. Takizawa, Y. Kuwata, M. Mutoh, N. Ishiguro, N. Utoguchi, A. Shinohara, M. Eriguchi, H. Yanagie, K. Maruyama, Effective anti-tumor activity of Oxaliplatin encapsulated in transferrin-PEG-liposome, Int. J. Pharm. 346 (2008) 143–150.
[59] L. Pendyala, Y. Kidani, R. Perez, J. Wilkes, R.J. Bernacki, P.J. Creaven, Cytotoxicity, cellular accumulation and DNA binding of oxaliplatin isomers, Cancer Lett. 97 (1995) 177–184.
[60] K.K. Sankhala, A.C. Mita, R. Adinin, L. Wood, M. Beeram, S. Bullock, N. Yamagata, K. Matsuno, T. Fujisawa, A. Phan, A phase I pharmacokinetic (PK) study of MBP-426, a novel liposome encapsulated oxaliplatin, J. Clin. Oncol. 27 (15 s) (2009) 2535.
[61] V.P. Torchilin, Passive and active drug targeting: drug delivery to tumors as an example, in: M. Schafer-Korting (Ed.), Handbook of Experimental Pharmacology, 197, Springer-Verlag, Berlin, 2010, pp. 4–36.